PNNL-13251

Pacific Northwest
National Laboratory
Operated by Battelle for the
U.S. Department of Energy

Preparation and Characterization of ^{238}Pu-Ceramics for Radiation Damage Experiments

D. M. Strachan
R. D. Scheele
W. C. Buchmiller
J. D. Vienna
R. L. Sell
R. J. Elovich

May 2000

Prepared for
the U.S. Department of Energy
under Contract DE-AC06-76RLO 1830

DISCLAIMER

PACIFIC NORTHWEST LABORATORY
operated by
BATTELLE MEMORIAL INSTITUTE
for the
UNITED STATES DEPARTMENT OF ENERGY
under Contract DE-AC06-76RLO 1830

Printed in the United States of America

Available to DOE and DOE contractors from the Office of Scientific and Technical Information, P.O. Box 62, Oak Ridge, TN 37831; prices available from (615) 576-8401.

Available to the public from the National Technical Information Service, U.S. Department of Commerce, 5285 Port Royal Rd., Springfield, VA 22161

DISCLAIMER

Portions of this document may be illegible in electronic image products. Images are produced from the best available original document.

PNNL-13251

Preparation and Characterization of ^{238}Pu-Ceramics for Radiation Damage Experiments

D. M. Strachan
R. D. Scheele
W. C. Buchmiller
J. D. Vienna
R. L. Sell
R. J. Elovich

May 2000

Prepared for
the U.S. Department of Energy
under Contract DE-AC06-76RLO 1830

Pacific Northwest Laboratory
Richland, Washington 99352

Summary

As a result of treaty agreements between Russia and the United States, portions of their respective plutonium and nuclear weapons stockpiles have been declared excess. In support of the U.S. Department of Energy's 1998 decision to pursue immobilization of a portion of the remaining Pu in a titanate-based ceramic, we prepared nearly 200 radiation-damage test specimens of five Pu- and ^{238}Pu-ceramics containing 10 mass% Pu to determine the effects of irradiation from the contained Pu and U on the ceramic. The five Pu-ceramics were 1) phase-pure pyrochlore [ideally, Ca(U, Pu)Ti_2O_7], 2) pyrochlore-rich baseline, 3) pyrochlore-rich baseline with impurities, 4) phase-pure zirconolite [ideally Ca(U, Pu)Ti_2O_7], and 5) a zirconolite-rich baseline. These ceramics were prepared with either normal weapons-grade Pu, which is predominately ^{239}Pu, or ^{238}Pu. The ^{238}Pu accelerates the radiation damage relative to the ^{239}Pu because of its much higher specific activity (651 TBq/kg [17.6 Ci/g] ^{238}Pu vs. 2 TBq/kg [0.06 Ci/g] ^{239}Pu). We were unsuccessful in preparing phase-pure (Pu, U) brannerite [(U, Pu)Ti_2O_6], which is the third crystalline phase present in the baseline immobilization form.

Since these materials will contain ~10 mass% Pu and about 20 mass% U, radiation damage to the crystalline structure of these materials will occur over time. As the material becomes damaged from the decay of the Pu and U, it is possible for the material to swell as the both the alpha particles and recoiling atoms rupture chemical bonds within the solid. As the material changes density, cracking, perhaps in the form of microcracks, may occur. If cracking occurs in ceramic that has been placed in a repository, the calculated rate of radionuclide release if the can has corroded would increase proportionately to the increase in surface area. This could lead to unacceptable radionuclide releases or to higher probabilities of nuclear criticality.

To investigate the effects of radiation damage on the five ceramics prepared, we are storing the specimens at 20, 125, and 250°C until the ^{238}Pu specimens become metamict, and the damage saturates. We will characterize and test these specimens every 6 months by 1) monitoring the dimensions, 2) monitoring the geometric and pycnometric densities, 3) monitoring the appearance, 4) determining the normalized amount leached during a 3-day, static, 90°C leach test in high purity water, and 5) monitoring the crystal structure with x-ray diffraction crystallography (XRD). In this paper, we document the preparation and initial characterization of the materials that were made in this study.

Our initial XRD characterizations indicate that the phase assemblages appear to be correct with the exception of the ^{238}Pu-zirconolite baseline material. We made this latter material using too much Pu, so this material contains unreacted PuO_2.

Our characterization of the physical properties of these materials found that the densities for all but three materials appear to be > 94% of theoretical, and only a few of the specimens have significant cracking. Those with cracking were the ^{239}Pu-zirconolite specimens, which were sintered with a heat-up rate of 5°C/min. We sintered the ^{238}Pu-zirconolite specimens with a heat-up rate of 2.5°C/min and obtained specimens with only minor surface cracking.

Elemental releases during our 3-day MCC leach tests show that the normalized elemental releases depend on 1) whether the Pu is ^{239}Pu or ^{238}Pu, 2) the material type, and 3) the identity of the constituent. The effect of the Pu isotope in the ceramic is most dramatic for Pu release, with nominally 50 to 100 times more Pu activity released from the ^{238}Pu specimens. This is unlikely to be an early indicator of radiation damage, because of the short time between specimen preparation and testing. In contrast, greater amounts of Mo are released from the ^{239}Pu specimens. The highest release levels are seen for the baseline materials. Of the contained constituents, Ca, Al, Pu, and U are the species found at relatively higher levels in the leachates.

Acknowledgments

The authors thank the following persons for their invaluable assistance in performing this work and preparing this report:

- Todd Schaef, Matt O'Hara, and Chris Brown for performing the inductively coupled plasma-atomic emission spectroscopy and inductively coupled plasma-mass spectrometry analyses.
- Richard Ratner, Larry Greenwood, and Kathy Thomas for performing the radiochemical analyses.
- Jonathan Icenhower, Henry Shaw (LLNL), and Rich Van Konynenburg (LLNL) for their technical reviews and comments.
- Wayne Cosby for performing an editorial review and preparing the document for production.

Pacific Northwest National Laboratory is operated for the U.S. Department of Energy by Battelle under Contract DE-AC06-76RLO 1830.

Contents

Tables

Figures

1.0 Introduction

As a result of treaty negotiations between Russia and the United States, portions of the plutonium and nuclear weapons stockpiles have been declared excess [1]. In January 2000, the U.S. Secretary of Energy recommended a dual-track approach to disposition approximately 50 metric tons of Pu [2]. In the first track, up to 33 metric tons of relatively clean Pu would be converted into mixed-oxide fuel that would then be irradiated in commercial light-water reactors. In the second track, a portion of the remaining Pu would be immobilized as a titanate-based ceramic. The ceramic would be placed in cans, and these cans would be further isolated by surrounding them with high-level nuclear waste glass. Research programs for both options have been ongoing for several years. With respect to immobilizing the dirty Pu, research is being carried out on the production and characterization of the ceramic material. The ceramic that was selected is a pyrochlore-based [ideally, (Ca, Gd, Hf, U, Pu)Ti_2O_7] ceramic containing ~10 mass% Pu. Characterization of this material has centered on elucidation of the relevant phase diagrams and the corrosion behavior of the material in contact with water.

The latter characteristic is important for the disposal of this material in a mined geologic repository. The only credible release of radionuclides from the repository to the accessible environment is when water contacts the disposed material and causes the release of the immobilized radionuclides, which are then transported in the aqueous phase. Because these materials contain ~10 mass% Pu and ~20 mass% U, radiation damage to the crystalline structure of these materials occurs over time. Disruption of the crystalline lattice causes an increase in the free energy of the material (i.e., energy is stored in the amorphous material). This increase in energy may lead to an increase in the corrosion rate. In addition, as the material becomes damaged from the decay of the Pu and U, it is possible for the material to swell [3]. Because each phase in the ceramic will contain differing concentrations of Pu and U, the phases will sustain damage at different rates and, hence, swell at different rates. In general, each phase will have a different final volume change. These changes may induce cracking, perhaps in the form of microcracks. If these microcracks form, the surface area available for contact by water will increase. This could lead to higher radionuclide releases or to higher probabilities of nuclear criticality [4].

Although the effects of radiation damage on other crystalline materials have been investigated [3, 5, 6, 7, 8, 9], the effects on some of the minerals that make up these ceramics have not. Furthermore, these effects have not been studied for phases having bulk chemical compositions similar to those in the Pu-ceramic; i.e., containing significant quantities of Gd, Hf, and U. Therefore, in 1996, research was initiated into the effects of radiation damage on pyrochlore ($CaUTi_2O_7$), zirconolite ($CaZrTi_2O_7$), brannerite (UTi_2O_6), and mixtures of the three. The Ca, U, and Zr sites in the respective crystal structures are heavily substituted with Gd, Hf, Pu, and other constituent metals in these ceramics [10]. In this paper, we document the preparation and initial characterization of the materials that were made in this study.

We begin by showing the test matrix that will be used throughout the study. This is followed by a discussion of the preparation of the materials and the characterization that took place at the time these materials were made. We then discuss the characterization of the materials as the testing began and end with some concluding remarks.

2.0 Test Matrix

The test matrix was developed with the intent of obtaining the maximum amount of information on the effects of radiation damage within the constraints of time and budget. There were to be six different materials plus two in which the microstructure had been coarsened by prolonged sintering at 1350°C. However, problems in making brannerite forced us to delete this material from the test matrix. Table 2.1 shows the test matrix for the seven materials to be studied. These materials are to be stored at three temperatures—ambient (~21°C), 125°C, and 250°C—to study the effect of temperature on the rate of damage in growth. If there is an observable effect, we will be able to calculate the temperature dependence of the damage annealing process.

The characterizations that we are performing to determine the effects of radiation damage from contained plutonium and uranium are determining 1) the bulk and pycnometric densities, 2) the mineral phases present by X-ray diffraction (XRD), 3) physical appearance, and 4) the amount of each component released during a modified Materials Characterization Center static leach test (MCC-1) [11]. These characterizations are sufficient to answer the main concerns with these ceramics as waste-form materials.

We are planning to perform modified MCC-1 tests [11] on most of these materials every 6 months, as the materials become metamict. The MCC-1 test is being used as a compromise between a number of different physical and chemical phenomena. A significant amount of radiolysis occurs to the aqueous solutions from the alpha activity associated with the ^{238}Pu. Radiolysis causes solutions to become more oxidizing, which could affect the rate at which elements, in particular Pu and U in the specimen, are released. The changing chemistry would make it very difficult to compare behaviors between specimens and between different materials. Limiting the duration of the test minimizes the radiolysis effects, but also limits the amount of material that dissolves, thereby affecting our ability to detect dissolved material. We decided that a 3-day MCC-1 test performed at 90°C with duplicate specimens would be of sufficient duration to give detectable amounts of material in solution while minimizing the effects of radiolysis. As part of another task at PNNL, we will study the effect of radiation damage on the dissolution of the material with a single-pass flow-through test [12, 13], but for one material only.

We analyzed the resulting MCC test solutions using inductively coupled plasma (ICP)- atomic emission spectroscopy (AES), ICP mass spectroscopy (MS), gamma energy analysis (GEA), and/or specific ion electrodes (SIE). The solutions resulting from the testing of the ^{239}Pu specimens were analyzed with both ICP/AES and ICP/MS while the solutions from the MCC tests of the ^{238}Pu specimens were analyzed with only ICP/MS because of the higher radioactivity levels. PNNL's radioanalytical group analyzed the ^{238}Pu solutions with GEA for released ^{238}Pu. Because we were using Teflon vessels, we analyzed all solutions with a fluoride SIE. The solutions resulting from the MCC testing of the baseline with impurities were analyzed for chloride with a chloride SIE. We measured pHs using a pH electrode. The fluoride, chloride, and pH calibration solutions were either NIST-traceable or prepared from NIST-traceable standards. Because of the overlap in the mass spectra of ^{238}Pu and ^{238}U, we calculated the ^{238}Pu concentration using the Pu's historical mass isotopics and the ICP/MS-measured ^{239}Pu. We then summed the ^{238}Pu and ^{239}Pu to provide the total chemically-determined Pu. The calculated ^{238}Pu was used to adjust the mass 238 amount to provide the ^{238}U. As will be illustrated later,

there is strong agreement between the ICP/MS-measured amounts of Pu and ^{238}Pu released in the MCC test.

Table 2.1. Radiation Damage Test Matrix

	Specimens in Storage								
	Storage Temperature								
Material	Ambient			125°C			250°C		
	Cyl[1]	Pellets[2]	TC[3]	Cyl	Pellets	TC	Cyl	Pellets	TC
239 Pyrochlore	1	3		1	3		1	3	
239 Zirconolite	1	4		1	4		1	4	
239 Z-Baseline[4]	1	4		1	4		1	4	
239 P-Baseline	1	4		1	4		1	4	
239 I-Baseline	1	4		1	4		1	4	
239 C-Pyrochlore	1	2		1	3		1	3	
239 C-Zirconolite	1	3		1	3		1	3	
	Ambient			125°C			250°C		
	Cyl	Pellets	TC	Cyl	Pellets	TC	Cyl	Pellets	TC
238 Pyrochlore	1	4	2	1	4	1	1	4	1
238 Zirconolite	2	6	1	1	4	1	1	4	2
238 Z-Baseline	2	6	1	2	6		2	6	
238 P-Baseline	2	6	1	2	6	1	2	6	1
238 I-Baseline	1	4	1	1	2		1	4	1
238 C-Pyrochlore	2	6							
238 C-Zirconolite	1	4							

	Analyses								
	Period								
	XRD			MCC-1			Density[5]		
	Begin[6]	6 mo	12 mo	Begin	6 mo	End	Begin	6 mo	12 mo
239 Pyrochlore	1A,1B,1C		1A,1B,1C	2A,2B,2C		2A,2B,2C	2A,2B,2C		2A,2B,2C
239 Zirconolite	1A,1B,1C		1A,1B,1C	2A,2B,2C		2A,2B,2C	2A,2B,2C		2A,2B,2C
239 Z-Baseline	1A,1B,1C		1A,1B,1C	2A,2B,2C		2A,2B,2C	2A,2B,2C		2A,2B,2C
239 P-Baseline	1A,1B,1C		1A,1B,1C	2A,2B,2C		2A,2B,2C	2A,2B,2C		2A,2B,2C
239 I-Baseline	1A,1B,1C		1A,1B,1C	2A,2B,2C		2A,2B,2C	2A,2B,2C		2A,2B,2C
239 C-Pyrochlore	1A,1B,1C		1A,1B,1C	2A,2B,2C		2A,2B,2C	2A,2B,2C		2A,2B,2C
239 C-Zirconolite	1A,1B,1C		1A,1B,1C	2A,2B,2C		2A,2B,2C	2A,2B,2C		2A,2B,2C
	XRD			MCC-1			Density		
	Begin	6 mo	12 mo	Begin	6 mo	12 mo	Begin	6 mo	12 mo
238 Pyrochlore	1A,1B,1C	1A,1B,1C		2A,2B,2C	2A,2B,2C		2A,2B,2C	2A,2B,2C	
238 Zirconolite	1A,1B,1C	1A,1B,1C		2A,2B,2C	2A,2B,2C		2A,2B,2C	2A,2B,2C	
238 Z-Baseline	1A,1B,1C		1A,1B,1C	2A,2B,2C		2A,2B,2C	2A,2B,2C	2A,2B,2C	
238 P-Baseline	1A,1B,1C		1A,1B,1C	2A,2B,2C		2A,2B,2C	2A,2B,2C	2A,2B,2C	
238 I-Baseline	1A,1B,1C		1A,1B,1C	2A,2B,2C		2A,2B,2C	2A,2B,2C	2A,2B,2C	
238 C-Pyrochlore	1A,1B,1C		1A,1B,1C	2A,2B,2C		2A,2B,2C	2A,2B,2C		2A,2B,2C
238 C-Zirconolite	1A,1B,1C		1A,1B,1C	2A,2B,2C		2A,2B,2C	2A,2B,2C		2A,2B,2C

1) Number of storage containers with specimens.
2) Number of specimens in each storage container.
4) Z = Zirconolite; P = Pyrochlore; I = Impurities; C = Coarse grained.
5) Geometric and gas pycnometer measurements.
6) A = Ambient; B = 125°C; C = 250°C.

Bulk density and pycnometric density are measured for the specimens. The bulk density is determined from the dimensions of the specimen and its mass. Normal and digital calipers are used to measure the pellet dimensions. Three or four determinations of the pellet height and diameter are made and averaged. We assume that the specimen approximates a right circular cylinder. For most of the specimens, the goodness of this assumption is reflected in the standard deviations shown in Table 4.1. Gas pycnometer densities are measured with a He gas pycnometer (Micromeretics, AccuPyc 1330) operated in the high precision mode (0.01% precision) with a 10-mL specimen cell and a 1-mL specimen insert. This Pycnometric density measurement excludes the specimen open porosity that is captured in the geometric bulk density measurement, but includes the closed porosity of the specimen.

A test specimen of each material type is periodically mounted in a special specimen holder for x-ray diffraction (XRD) analysis to determine the mineral phases present in the specimen. The XRD pattern is obtained from a pellet surface that has been polished with 600-grit SiC paper. To calibrate the XRD instrument, a disk of NIST SRM 1976, that has been mounted permanently in an identical specimen holder, is analyzed daily when the Pu-bearing ceramic specimens are being analyzed. We use the SRM material as a position and intensity standard, although NIST supplies the SRM as an intensity standard.

Pictures were also taken of the specimens to monitor changes in physical appearance. We use a high-resolution video camera to capture the image on the computer. While the video camera does not give as high a resolution as a photographic film camera, the ease of use in the fume hood and the ease of obtaining the image outweigh the loss in resolution. The quality of these images is sufficient to document small cracks and chips in the original specimen pellets and subsequent physical changes that might occur as the specimens age.

As shown in Table 2.1, the specimens are to be stored at three different temperatures: ambient (~21°C), 125°C, and 250°C. Six to 9 thermocouples are placed in each oven, some in the base of selected ^{238}Pu-specimen storage vessels. The outputs from these thermocouples are routed to a multichannel multiplexing board with an electronic cold-junction compensator. The channels on the board are polled with a computer. Temperatures are recorded at least every hour, but, during some reviews, data may be collected every minute. The temperature data are saved to the computer hard drive and periodically stored on a compact disk.

Stainless steel vessels are used to store the test specimens between test periods. A photograph and schematic of a radiation damage specimen storage vessel are shown in Figure 2.1. In a typical ^{238}Pu vessel, one or two pellets which have been polished with 600-grit SiC paper on both sides is/are sandwiched between two pellets which have been polished on a single side. Only polished faces are in contact with one another to ensure that the interfaces will be similar to a pellet's interior and will experience maximum radiation damage. The ^{239}Pu pellets are placed in a similar vessel, however, the ^{239}Pu pellets are not held firmly in position because little radiation damage will occur in these specimens. Selected vessels containing the ^{238}Pu specimens have thermocouple wells in the base near the specimens. This allows the temperature of the vessel to be monitored and any increase in temperature due to radiodecay heat to be measured.

The vessels holding the ^{238}Pu specimens have stainless steel closure fixtures while the vessels holding the ^{239}Pu specimens have brass closure fixtures. The closure fixtures for the vessels holding the ^{238}Pu specimens are tightened to 150 ft-lbs by use of a torque wrench while the vessels holding the ^{239}Pu specimens are tightened with standard wrenches.

After tightening, each of the vessels is evacuated and back-filled with argon gas three times before the vent closure is sealed with cap. This should prevent any effects due to radiolysis of moisture and/or the air. Radiolysis of the air can cause the formation of NO_x and, in the presence of moisture, HNO_3 that can subsequently attack and degrade the specimens.

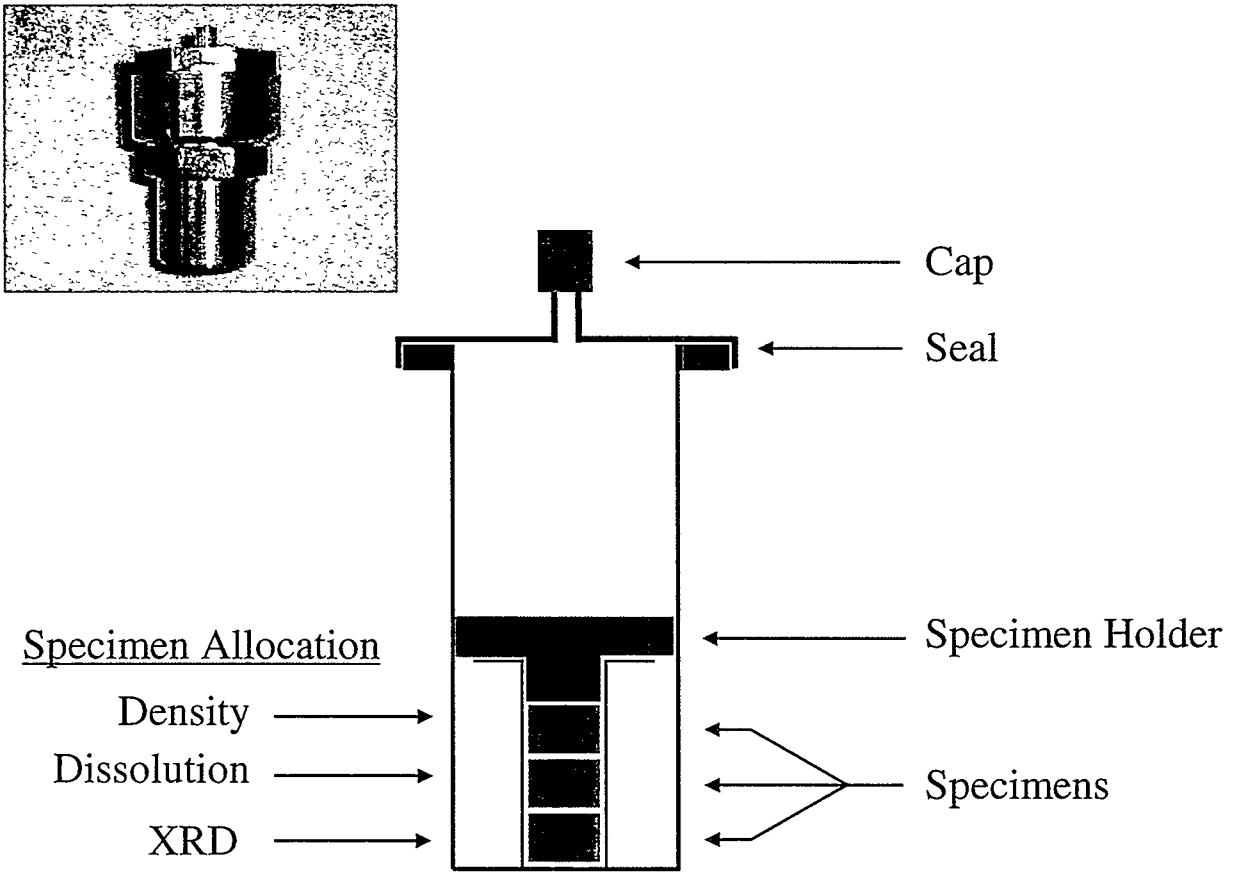

Figure 2.1. Photograph and Schematic of Radiation Damage Test Specimen Storage Vessel

3.0 Materials Preparation

As a precursor to preparing the Pu-containing specimens, we prepared several materials with Ce to develop the appropriate recipes and preparation conditions for the Pu-ceramics. Cerium is often used as a non-radioactive surrogate for Pu because of cerium's similar chemistry. We successfully prepared each of the target Ce-ceramics; however, we often had to revise our target compositions and preparation conditions. We will discuss the preparation of the Ce-ceramics in a separate document. Here, we will discuss the methods that were used to prepare the materials for the radiation-damage study and will provide the make-up compositions. Actual bulk chemical analyses of the final Pu-ceramics were not performed. Experience from the non-radioactive sample preparation indicated that the target (as-batched) and analyzed compositions were very close.

To form the primary mineral phases and the molybdenum tracer in our ceramics, we began with reagent-grade powdered $Al(OH)_3$, CaO or $Ca(OH)_2$, Gd_2O_3. HfO_2, MoO_3, and TiO_2 (Anatase); we used UO_2 available in the laboratory. The Pu was added as a nitric acid solution having a measured concentration. The preparation of the ^{238}Pu specimens was complicated by high specific activity of the Pu coupled with its high-heat production and resulting radiolysis and evaporation of water; Pu solutions are not stored in sealed containers for safety reasons. The loss of water from the ^{238}Pu solutions was accommodated in most cases, except for the ^{238}Pu-zirconolite-rich baseline material, which resulted in excess PuO_2. For the impure baseline ceramic, we added reagent-grade powders of H_3BO_3, $CaCl_2$, Cr_2O_3, Fe_2O_3, Ga_2O_3, K_2CO_3, MgO, Na_2CO_3, NiO, SiO_2, Ta_2O_5, WO_3, ZnO, and 98% CaF_2 as sources of the impurities. We prepared the ^{239}Pu specimens using $Ca(OH)_2$ as our source of Ca with the exception of the pyrochlore. The ^{239}Pu pyrochlore and all the ^{238}Pu specimens were prepared with CaO that was made by calcining reagent grade $Ca(OH)_2$ at 800°C to a constant mass. This CaO was subsequently stored in a dessicator with a desiccant.

Bench instructions were prepared for each batch of ceramic to be prepared, and the calculations were independently checked. We prepared 40- to 50-g batches of ^{239}Pu-containing ceramics and 5- to 15-g batches of the ^{238}Pu-containing ceramics from the starting materials and the appropriate volume of Pu stock solution. About 100 g of H_2O was added to the mixture, and the mixture was quantitatively transferred to a polyethylene bottle containing about 1000 g (^{239}Pu-ceramics) and 200 to 350 g (^{238}Pu-ceramics) of yttria-stabilized zirconia media. The zirconia media were "rounded" right circular cylinders about 6 mm in diameter by about 12 mm in height. The "ball milling jar" was placed on a roller, and the mix was milled for 2 h for the ^{239}Pu-ceramics, except pyrochlore, and a minimum of 16 h for the ^{238}Pu-ceramics and the ^{239}Pu pyrochlore.

After milling, the mixture was placed on a coarse screen to remove the milling media. The slurry was allowed to fall into a beaker. The residual slurry was washed from the media with demineralized water. The slurry was heated at slightly less than boiling to thicken in the beaker with constant stirring. When the magnetic stir bar would no longer turn because the viscosity of the slurry was too high, the stir bar was removed, and the beaker was transferred to an oven maintained at 110°C. Once the slurry had dried, it was pressed through a coarse screen, pressed into a single pellet, and crushed through a screen. The resulting powder was pressed into pellets that were about 3–4 mm in height for the ^{239}Pu-ceramic

specimens and 2–3 mm in height for the ^{238}Pu-ceramic specimens. Each pressed pellet was 12.5 mm in diameter.

At the start of the project, there were plastic windows in the glove box where these preparations were taking place. Because of fire concerns, this limited the time during which the ^{239}Pu specimens could be sintered to 8 to 10 h from the start of the cycle until the furnace was switched off. Heating rates up to 10°C/min were used to reach the 1350 to 1400°C sintering temperatures in the allowable time. Therefore, some of the initial ^{239}Pu specimens that were made were highly cracked and were returned to the milling step, repressed, and then resintered at a slower heating rate of 5 or 2.5°C/min. Later, glass windows were installed in the glove box, and the sintering furnace could remain on while unattended.

We sintered the specimens for 4 to 8 h at 1350°C in Ar with the exceptions of the ^{239}Pu- and ^{238}Pu-zirconolites, which we fired at 1400°C, and the ^{238}Pu zirconolite-rich baseline ceramic, which we sintered for 12 h. Initially, the unsintered specimens were placed on a platinum foil in the furnace. Later, some cerium pyrochlore-rich baseline ceramic was ground and placed on the foil to prevent the pellets from sticking. Initially, argon gas was directed toward the specimens through a ceramic tube. For most of the ^{238}Pu-ceramic specimens, a mullite crucible was inverted over the specimens, and the Ar gas was admitted through a ceramic tube in a hole in the floor of the furnace. The latter configuration, while still not perfect, gave better control over the sintering atmosphere.

To prepare the coarse pyrochlore and zirconolite specimens, we sintered specimens from the prepared pyrochlores and zirconolites for an additional 110 h at 1350°C.

The target compositions for the ^{238}Pu- and ^{239}Pu-ceramic specimens are shown in Table 3.1 and Table 3.2, respectively. Table 3.3 lists the components and amounts that make up the impurities for the impure baseline materials. Two batches of the ^{238}Pu-pyrochlore ceramic were made. The reason for making two batches was logistic rather than technical.

Table 3.1. Compositions of the ^{238}Pu-Ceramics Used in this Study. See Table 3.3 for the components and amounts of the impurities in the impure baseline material. Two batches of pyrochlore were made.

Component	^{238}Pu-Pyrochlore		^{238}Pu-Pyrochlore		^{238}Pu-Pyrochlore Baseline	
	mass%	mol %	mass%	mol %	mass%	mol %
Al_2O_3	0.00	0.00	0.00	0.00	0.00	0.00
CaO	12.06	24.89	12.53	25.05	9.91	21.13
Gd_2O_3	7.65	2.44	7.96	2.46	7.95	2.62
HfO_2	10.88	5.98	11.30	6.02	9.61	5.46
TiO_2	36.17	52.39	37.58	52.72	36.70	54.89
PuO_2	12.31	5.27	11.27	4.68	11.84	5.24
UO_2	20.82	8.93	19.24	8.98	23.88	10.57
MoO_3	0.10	0.09	0.12	0.09	0.11	0.10

Component	^{238}Pu-Impure Baseline		^{238}Pu-Zirconolite		^{238}Pu-Zirconolite Baseline	
	mass%	mol%	mass%	mol%	mass%	mol%
Al_2O_3	0.50	0.58	1.74	1.97	1.74	1.97
CaO	9.44	19.95	10.20	21.03	10.20	21.03
Gd_2O_3	7.54	2.47	2.06	0.66	2.06	0.66
HfO_2	10.07	5.67	43.08	23.66	43.08	23.66
TiO_2	34.03	50.51	33.61	48.63	33.61	48.63
PuO_2	11.26	4.94	7.40	3.17	7.40	3.17
UO_2	22.57	9.91	1.81	0.79	1.81	0.79
MoO_3	0.28	0.26	0.10	0.09	0.10	0.09
Impurities	4.33	5.71				

Table 3.2. Compositions of the ^{239}Pu-Ceramics Used in this Study. See Table 3.3 for the components and amounts of the impurities in the impure baseline material.

Component	^{239}Pu-Pyrochlore		^{239}Pu-Pyrochlore Baseline		^{239}Pu-Impure Baseline	
	mass%	mol %	mass%	mol %	mass%	mol%
Al_2O_3	0.00	0.00	0.00	0.00	0.50	0.58
CaO	12.07	24.91	9.94	21.15	9.20	19.47
Gd_2O_3	7.64	2.44	7.94	2.61	7.62	2.49
HfO_2	10.88	5.98	9.63	5.46	10.21	5.76
TiO_2	36.15	52.38	36.82	54.99	34.38	51.06
PuO_2	12.35	5.27	11.88	5.23	10.83	4.74
UO_2	20.82	8.92	23.67	10.46	22.70	9.98
MoO_2	0.10	0.09	0.10	0.10	0.27	0.25
Impurities					4.30	5.66

Component	^{239}Pu-Zirconolite		^{239}Pu-Zirconolite Baseline	
	mass%	mol%	mass%	mol%
Al_2O_3	1.88	2.13	1.13	1.35
CaO	10.18	20.99	9.22	19.94
Gd_2O_3	2.06	0.66	6.60	2.21
HfO_2	43.01	23.63	24.18	13.92
TiO_2	33.56	48.57	33.82	51.31
PuO_2	7.39	3.15	9.56	4.28
UO_2	1.83	0.79	15.38	6.90
MoO_2	0.10	0.09	0.10	0.09

Table 3.3. A List of the Components and Amounts of the Impurities in the ^{238}Pu- and ^{239}Pu-Impure Baseline Ceramics Shown in Table 3.1 and Table 3.2

Component	^{238}Pu-Impure Baseline		^{239}Pu-Impure Baseline	
	mass%	mol%	mass%	mol%
B_2O_3	0.17	0.29	0.15	0.25
$CaCl_2$	0.66	0.71	0.67	0.71
CaF_2	0.44	0.67	0.44	0.67
Cr_2O_3	0.09	0.07	0.09	0.07
Fe_2O_3	0.15	0.11	0.15	0.11
Ga_2O_3	0.57	0.36	0.57	0.36
K_2O	0.32	0.40	0.33	0.42
MgO	0.44	1.29	0.44	1.29
Na_2O	0.14	0.26	0.12	0.23
NiO	0.13	0.21	0.13	0.21
SiO_2	0.46	0.90	0.46	0.92
Ta_2O_3	0.19	0.05	0.19	0.05
WO_2	0.49	0.27	0.49	0.27
ZnO	0.07	0.11	0.07	0.10

4.0 Results from the Initial Characterization

Specimens were characterized from December 1999 through January 2000. Only the specimens stored at ambient temperature were characterized. This was valid because these specimens were selected randomly from the batch of specimens that were produced and, hence, adequately represent all specimens used in the radiation damage experiments.

4.1 Specimen Density

Specimen geometric densities were determined from the specimen mass and the measured geometric volume. Obtaining consistent measurements of the height and diameter in the glove box proved quite challenging. This is because it is difficult to properly align the caliper heads on the specimen surfaces. While this usually leads to a low density, high values for the density may also result if low values of the specimen dimensions are read. This can be the result of exerting too much pressure on the caliper jaws. Discrepancies were noted between the measurements made during the production and during this initial characterization. Several checks of the data were needed to resolve these inconsistencies. A consistent set of densities is shown in Table 4.1. The densities of the specimens should not have changed between the time they were polished and the time the first characterization was completed. However, it was decided that several densities of the ^{238}Pu-bearing specimens should be spot-checked. These data are shown under the "Initial Characterization" column in Table 4.1. For those pellets, the density that was determined at the time the specimens were polished is shown in the "Production" column. The average density for each material for all specimens produced is also shown.

Determining the geometric densities of these specimens in a glove box while manipulating both the specimen and the calipers with heavy gloves on one's hands leads to large errors in the determination of the dimensions. The Applied Physics group at Pacific Northwest National Laboratory (PNNL) is developing an inexpensive, automated method for measuring the dimensions of the specimens. This method should remove most of the uncertainties and subjectivity of the measurements.

Helium pycnometer densities are also shown in Table 4.1. These pycnometric densities are more reliable because only the specimen's mass is needed as input to the gas pycnometer. The program for the gas pycnometer is set to run in the high precision mode in which the density is recorded after five successive measurements of the specimen volume differ from one another by less than 0.01%.

Table 4.1. Geometric and Gas Pycnometric Densities for Radiation-Damage Test Specimens

Materials	Density (kg/m^3, x 10^{-3})			
	Geometric			Pycnometric
	Average	Production	Initial Characterization	Initial Characterization
239 Pyrochlore	5.31(4)[(a)]			5.54(1)
239 Zirconolite	5.15(4)			5.62(1)
239 P-Baseline	5.38(3)			5.78(1)
239 Z-Baseline	5.30(8)			5.61(1)
239 I-Baseline	5.38(3)			5.55(1)
239C-Pyrochlore	5.46(7)			5.43(1)
239C-Zirconolite	5.27(3)			5.68(2)
238 Pyrochlore	5.50(5)	4.91	5.38(12)	5.32(1)
		5.53	5.33(12)	
			5.33(13)	
		5.54	5.39(9)	
238 Zirconolite	5.17(5)		5.36(3)	5.76(1)
238 P-Baseline	4.77(5)		4.76(3)	5.49(1)
238 Z-Baseline	6.79(19)			6.33(1)
238 I-Baseline	5.26(6)			5.02(1)
238C-Pyrochlore	4.81(8)		4.75(10)	4.71(1)
238C-Zirconolite	5.23(34)	4.97	5.21(18)	5.42(1)
		5.69	5.13(25)	
		5.21	5.20(9)	
		5.05	4.81(15)	

(a) The number in () is the uncertainty in the last place as determined from three or four measurements of the dimensions. The uncertainty in the average is from all measurements made for that material. The uncertainty in the gas pycnometer density is in the third decimal place, but only two are reported. In this case, the value was rounded up to (1).

The gas pycnometric density should be greater than the geometric density because open porosity and cracks are included in the geometric measurement. In several cases, the gas pycnometric density of a ceramic is less than its measured geometric density. In the cases where the pycnometric density is less than the geometric density, the gas pycnometric density is probably the more reliable measurement because of difficulties measuring the dimensions of a pellet with calipers in a glove box. Hence, the gas pycnometric density should be taken as the value for both the geometric and gas densities for those specimens where the measured geometric density is less than the gas density. That is, there is probably no measurable open porosity in these specimens. This appears to be a valid conclusion based on a comparison with theoretical densities. When compared with rough theoretical densities reported by Stewart, Vance, and Ball [14], the gas pycnometric densities are greater than 94% of theoretical. There are three exceptions, 238 Z-Baseline (108%), 238 I-Baseline (85%), and 238 C-Pyrochlore (80%). For densities that are greater than about 90% of theoretical, almost the entire porosity is closed [15]. Therefore, the gas and bulk densities should be nearly the same.

In general, there is more variability in the densities of the ^{238}Pu- ceramic specimens than the ^{239}Pu-specimens. This is surprising because great care was taken to make sure that the conditions for successfully making the ^{239}Pu-bearing ceramic specimens were duplicated when making the ^{238}Pu-ceramic specimens. It also appears that coarsening the microstructure by sintering the ceramic for an additional 110 h at 1350°C generally caused the density to decrease.

4.2 Specimen Mineralogy (X-Ray Diffraction)

We used XRD to determine the mineral phases present in both the ^{239}Pu- and ^{238}Pu-ceramics. The ^{239}Pu-ceramics were analyzed immediately after production to ensure that we had successfully made the target ceramic. Selected specimens of the ^{238}Pu-ceramics were characterized as part of the initial characterization.

After preparing the ^{239}Pu-bearing specimens, we submitted powdered fragments for XRD analyses. These results are shown in Figure 4.1 through Figure 4.6. An analysis of the coarse zirconolite ceramic was not obtained. In each of the figures, "stick" patterns are included. In black and white, it is not possible to distinguish between the different "stick" patterns. Therefore, a letter marker is placed above the major peaks to identify each phase. In the ^{239}Pu-bearing zirconolite (Figure 4.2), some diffraction peaks are split. This might be due to incomplete reaction of the starting materials. In the next characterization of these materials, the coarse zirconolite will be examined to determine if the additional sintering that these specimens received decreased the splitting of the peaks. Since there are several polytypes for zirconolite, splitting of the peaks may be the result of inadequate sintering to remove all but the "2M" polytype. The additional peaks that are found in the ^{239}Pu-bearing baseline materials are from brannerite. These peaks were not labeled and the "stick" patterns were omitted for clarity reasons.

Figure 4.7 through Figure 4.13 show the results from the XRD analyses of the ^{238}Pu-bearing specimens. These figures provide XRD analyses of polished specimens. As with the ^{239}Pu-bearing materials, the ^{238}Pu-bearing baseline materials contained the target phases, except for the zirconolite

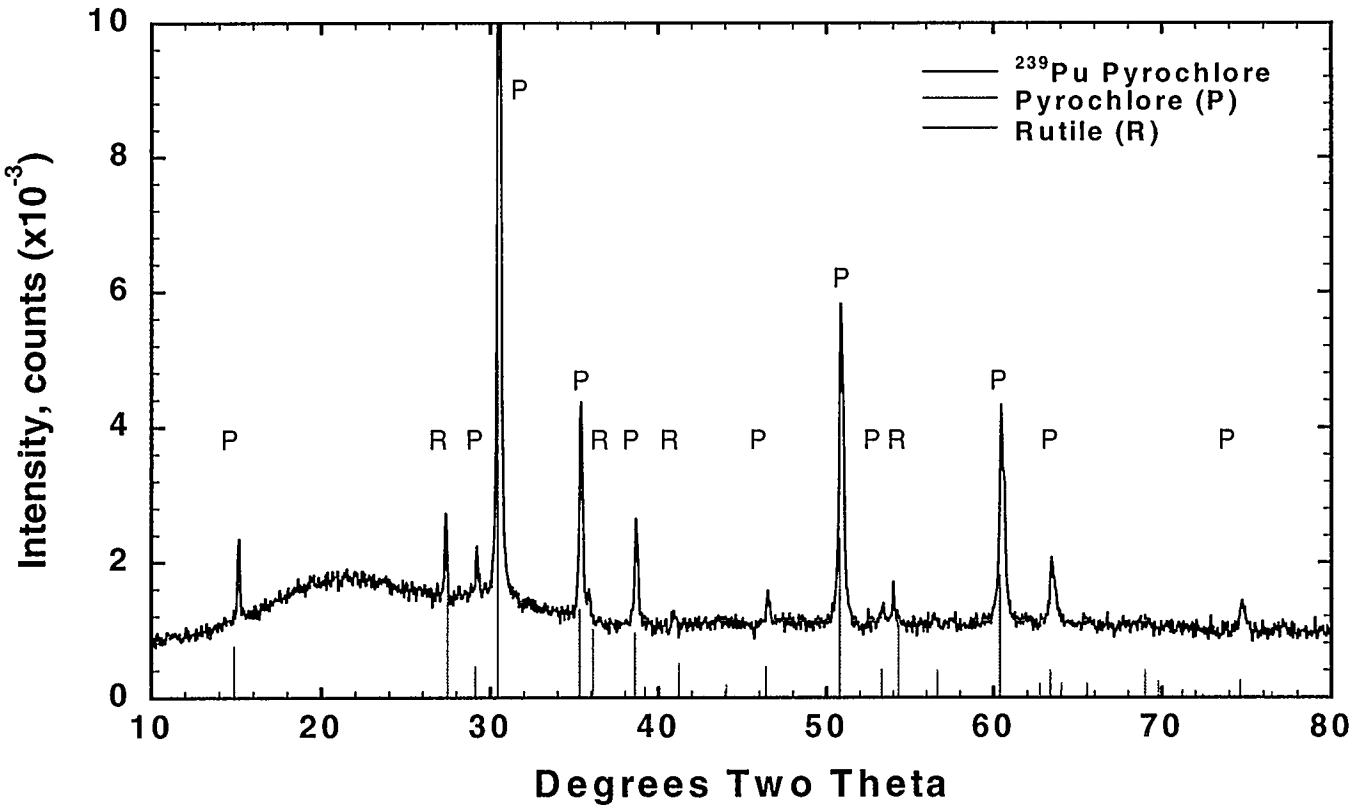

Figure 4.1. Results from the XRD Analysis of ^{239}Pu Pyrochlore

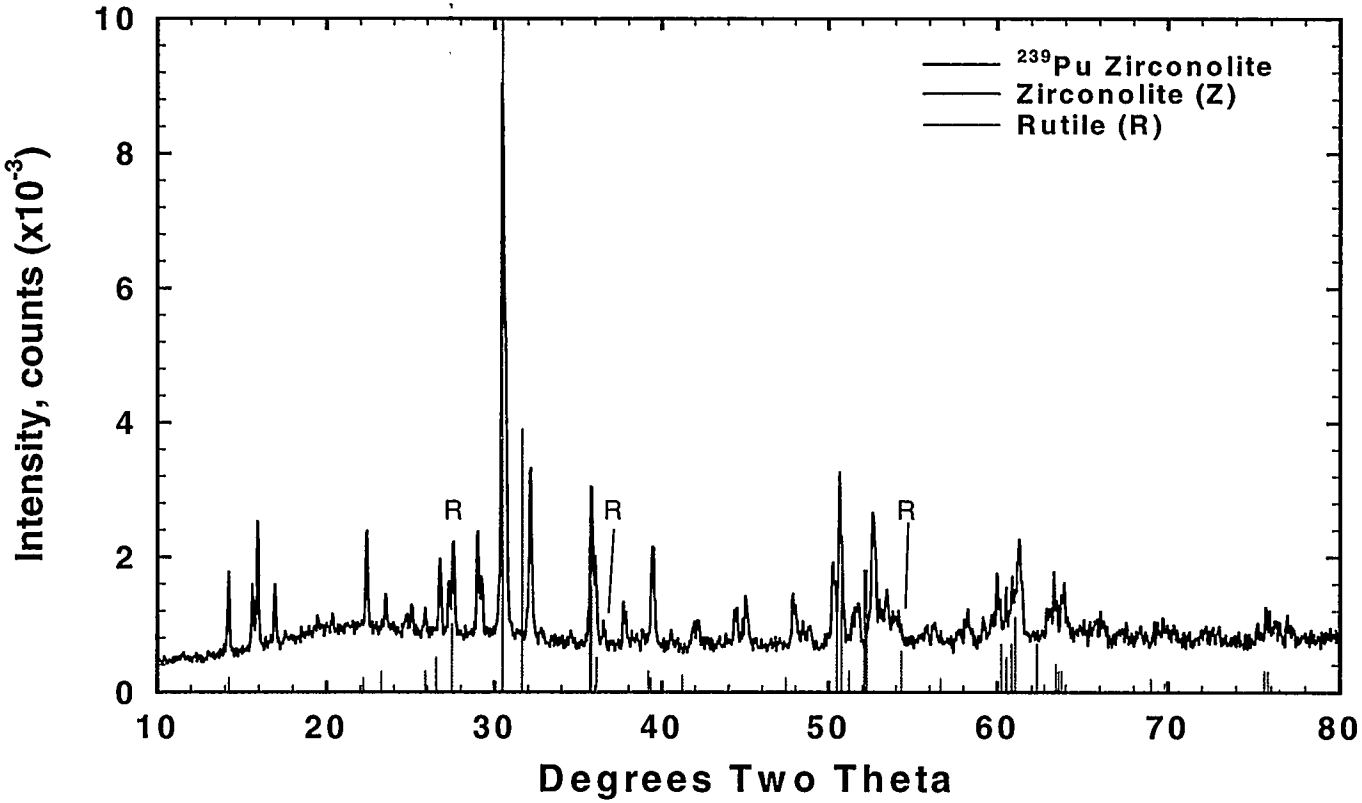

Figure 4.2. Results from the XRD Analysis of ^{239}Pu Zirconolite

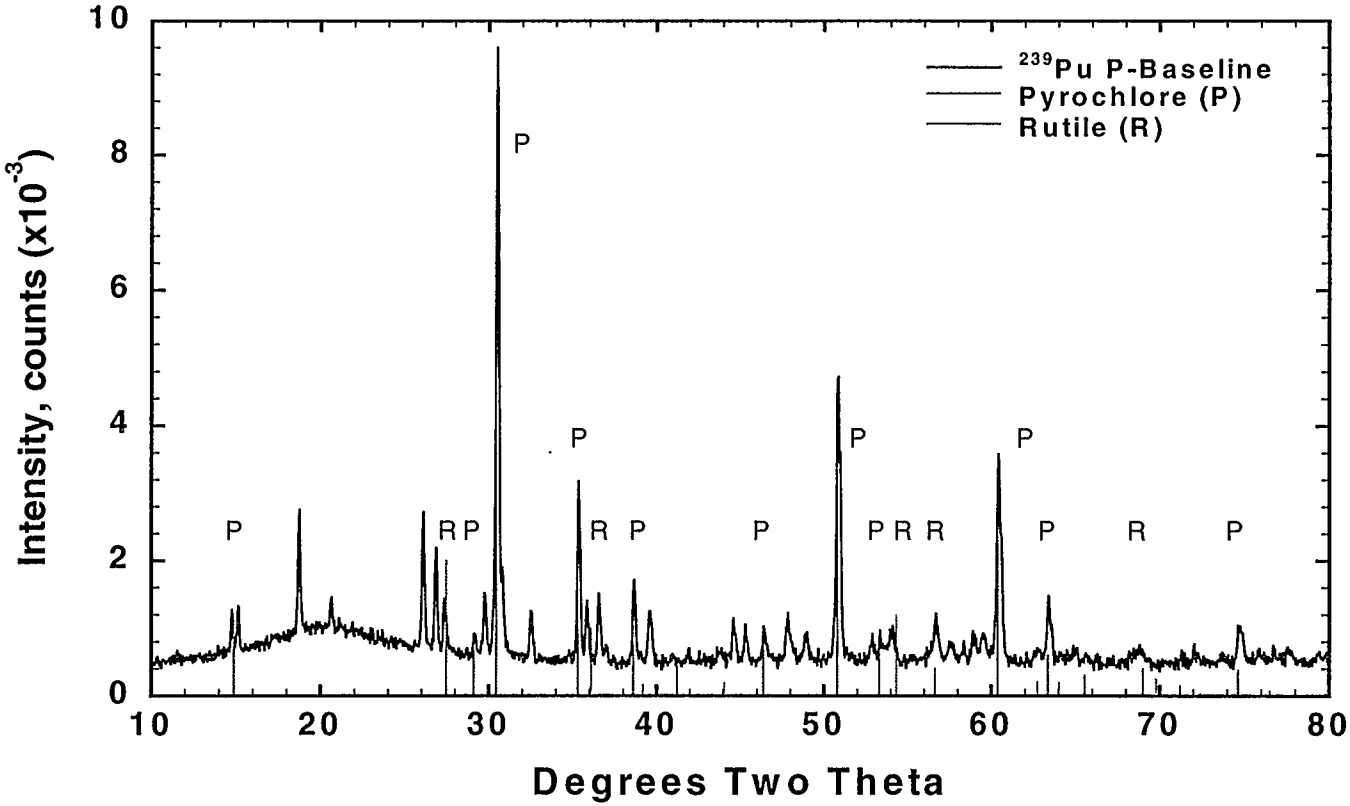

Figure 4.3. Results from the XRD Analysis of ^{239}Pu Pyrochlore Baseline

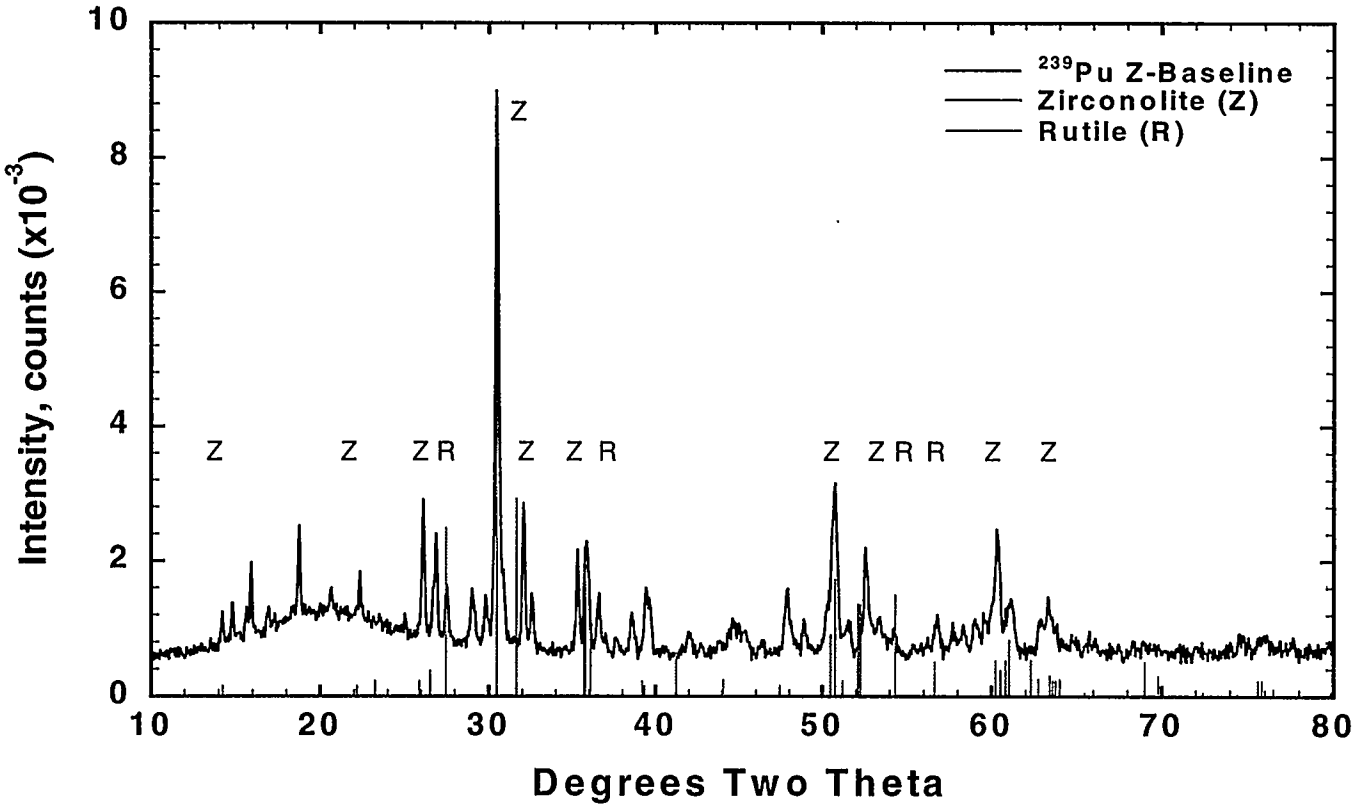

Figure 4.4. Results from the XRD Analysis of ^{239}Pu Zirconolite Baseline

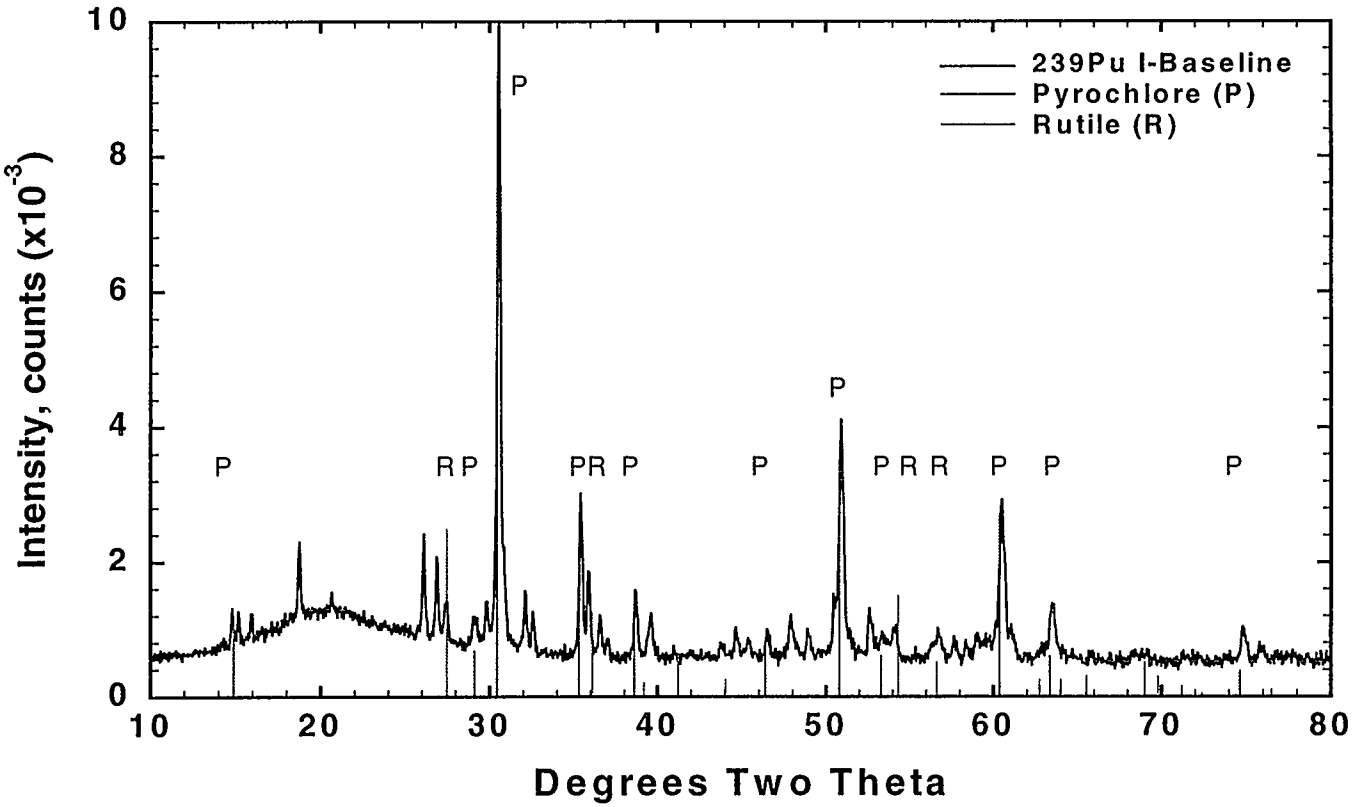

Figure 4.5. Results from the XRD Analysis of ^{239}Pu Impure Baseline

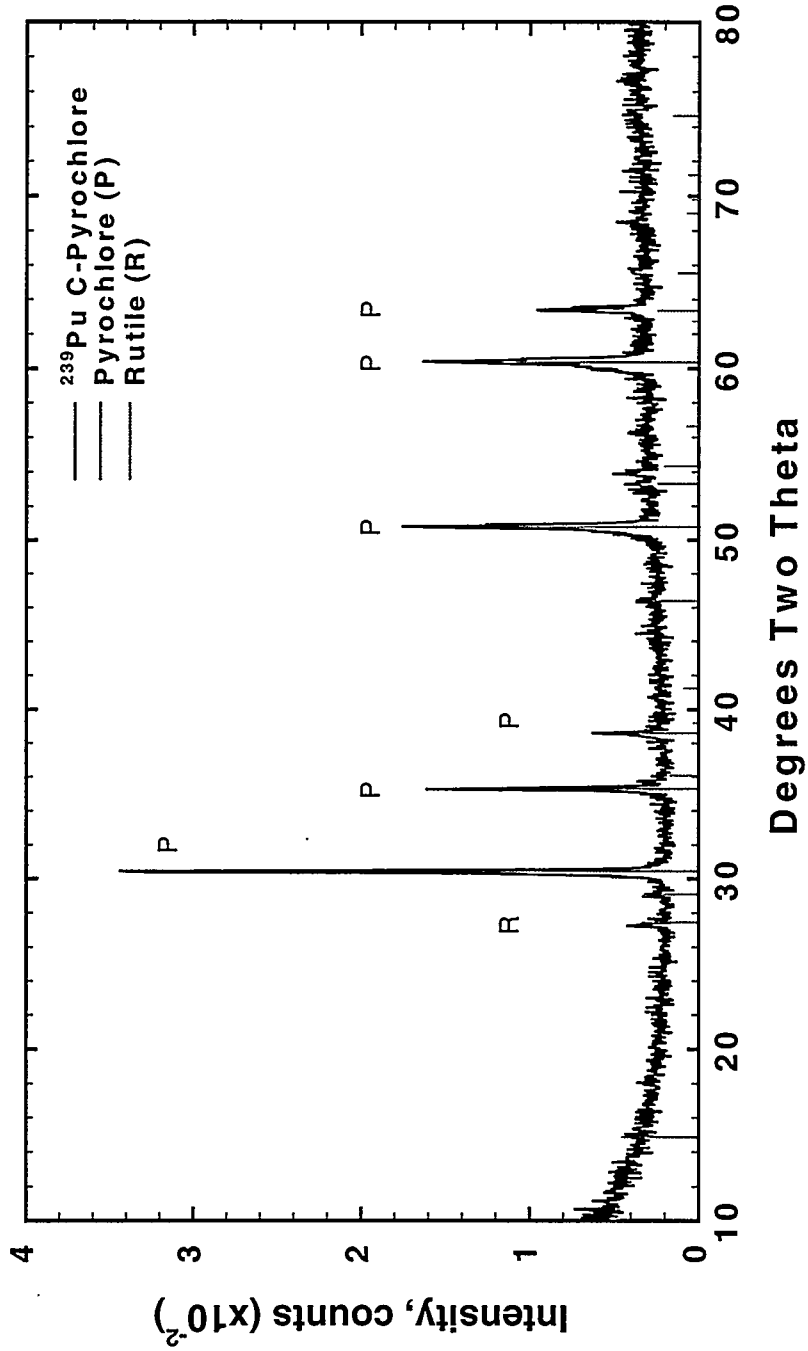

Figure 4.6. Results from the XRD Analysis of ^{239}Pu Coarse Pyrochlore

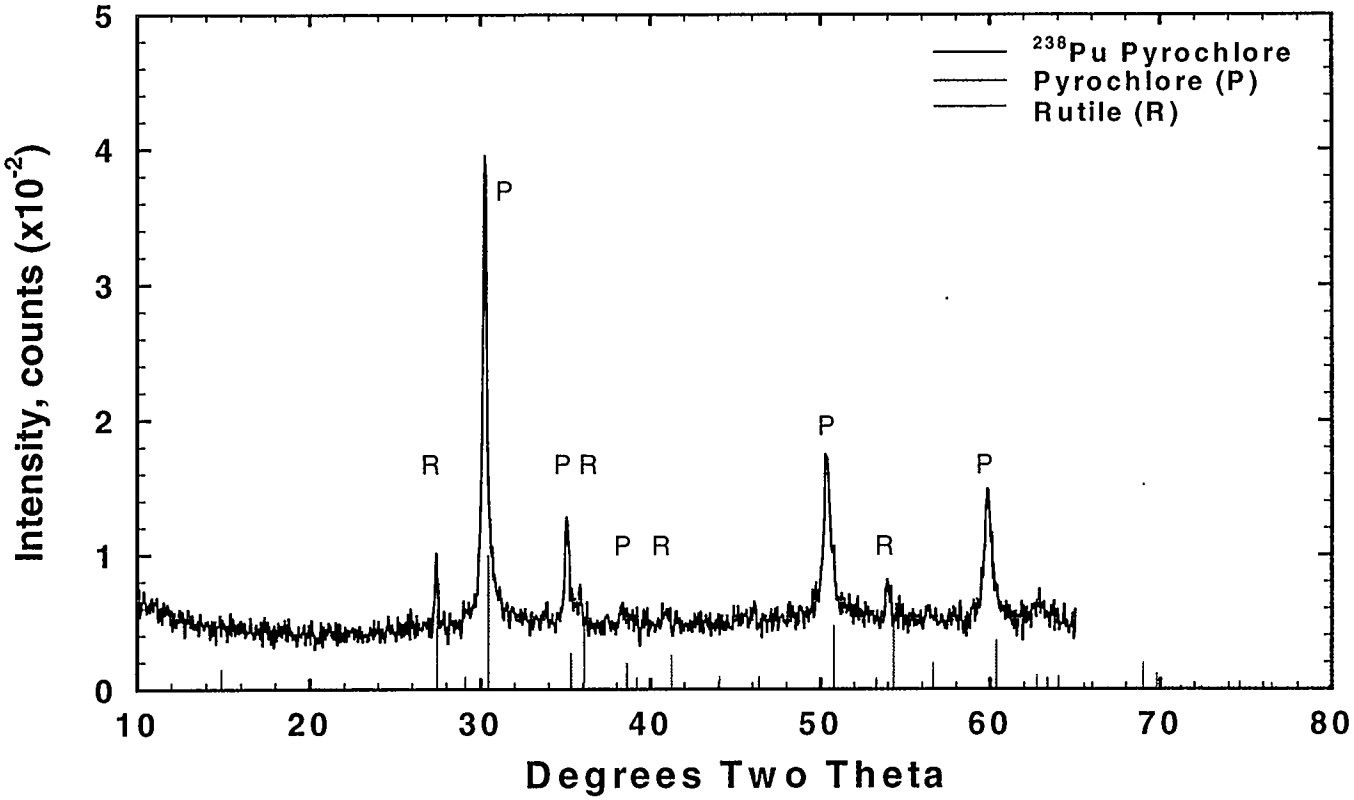

Figure 4.7. Results from the XRD Analysis of ^{238}Pu Pyrochlore

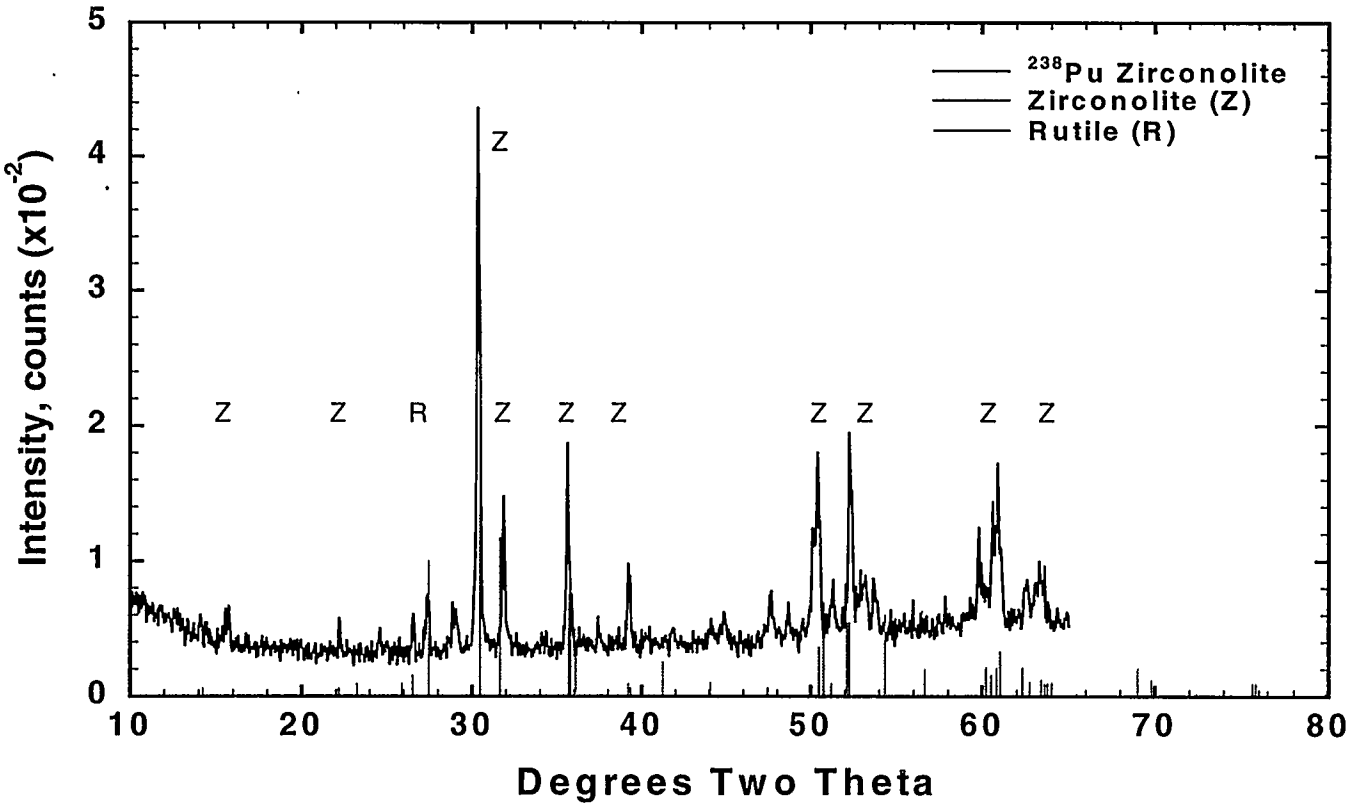

Figure 4.8. Results from the XRD Analysis of ^{238}Pu Zirconolite

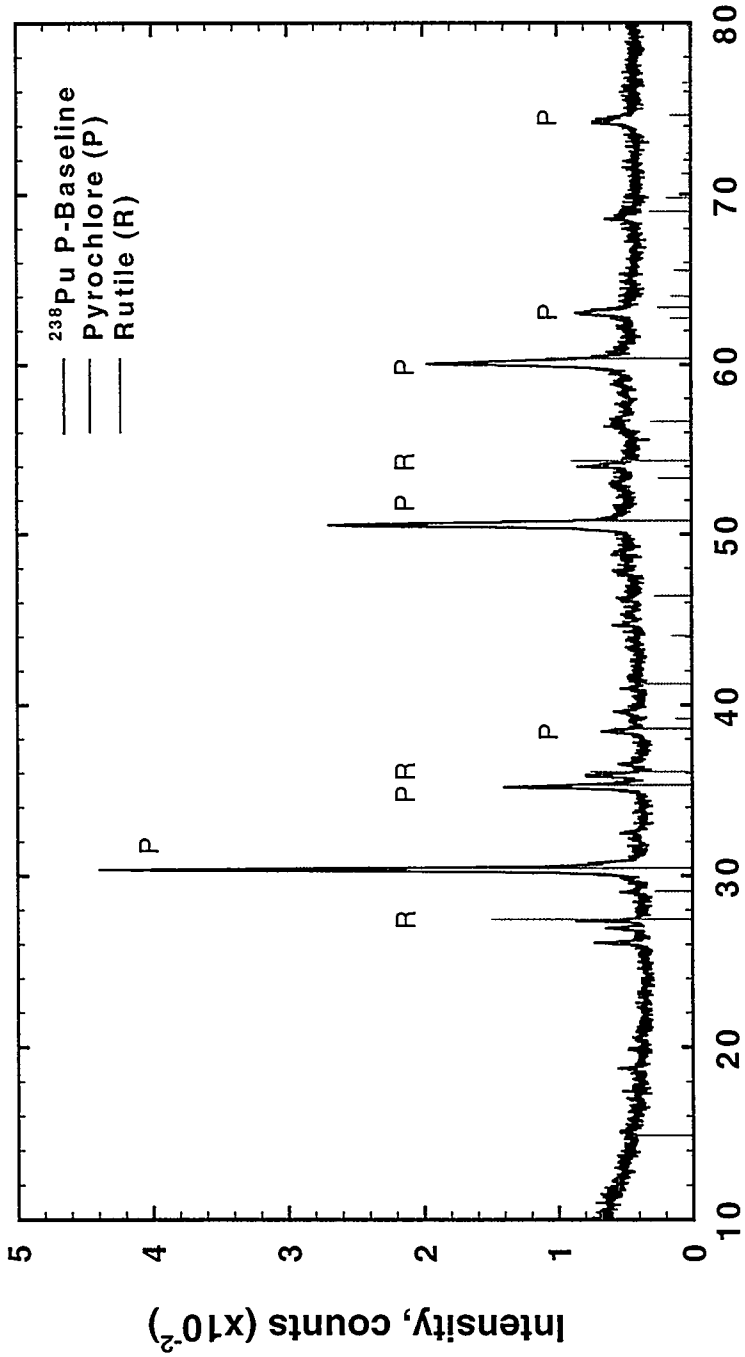

Figure 4.9. Results from the XRD Analysis of ^{238}Pu Pyrochlore Baseline

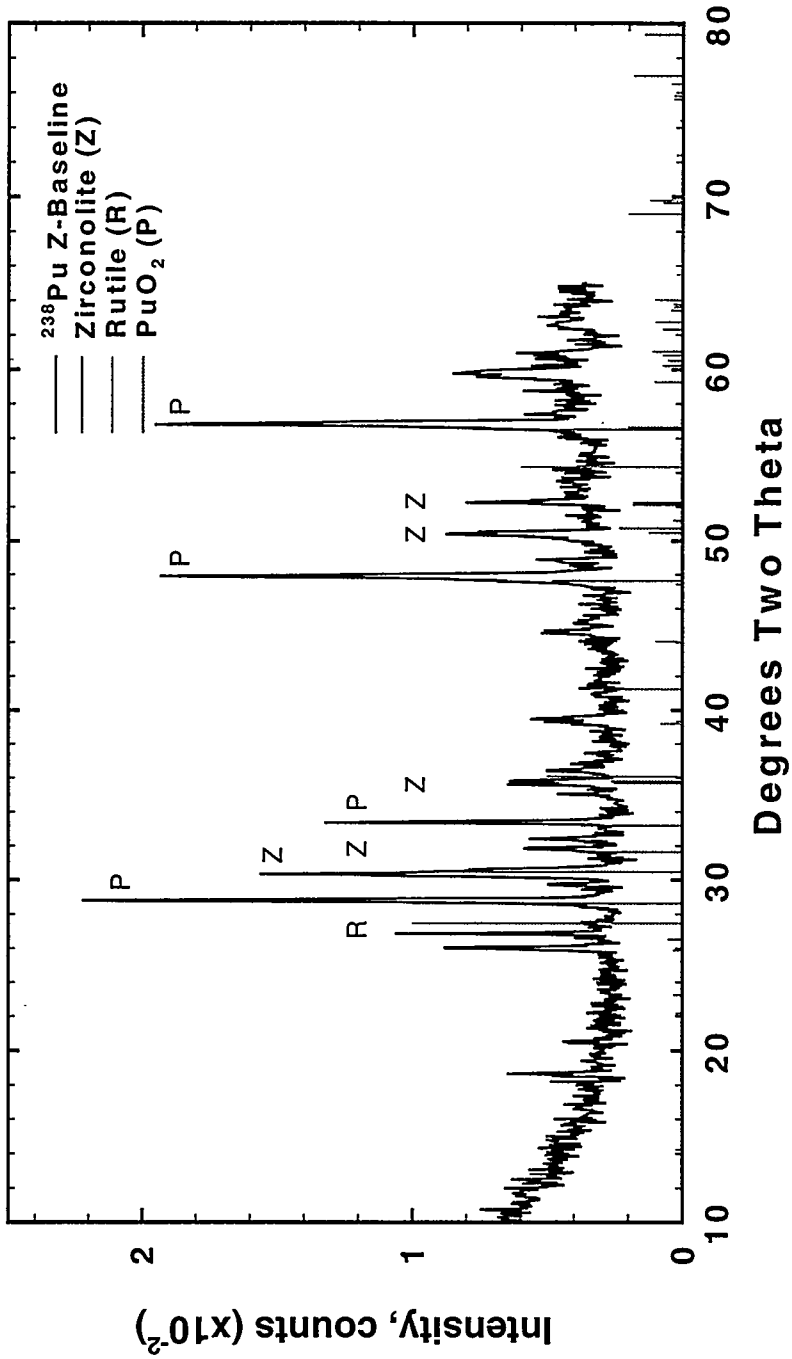

Figure 4.10. Results from the XRD Analysis of ^{238}Pu Zirconolite Baseline

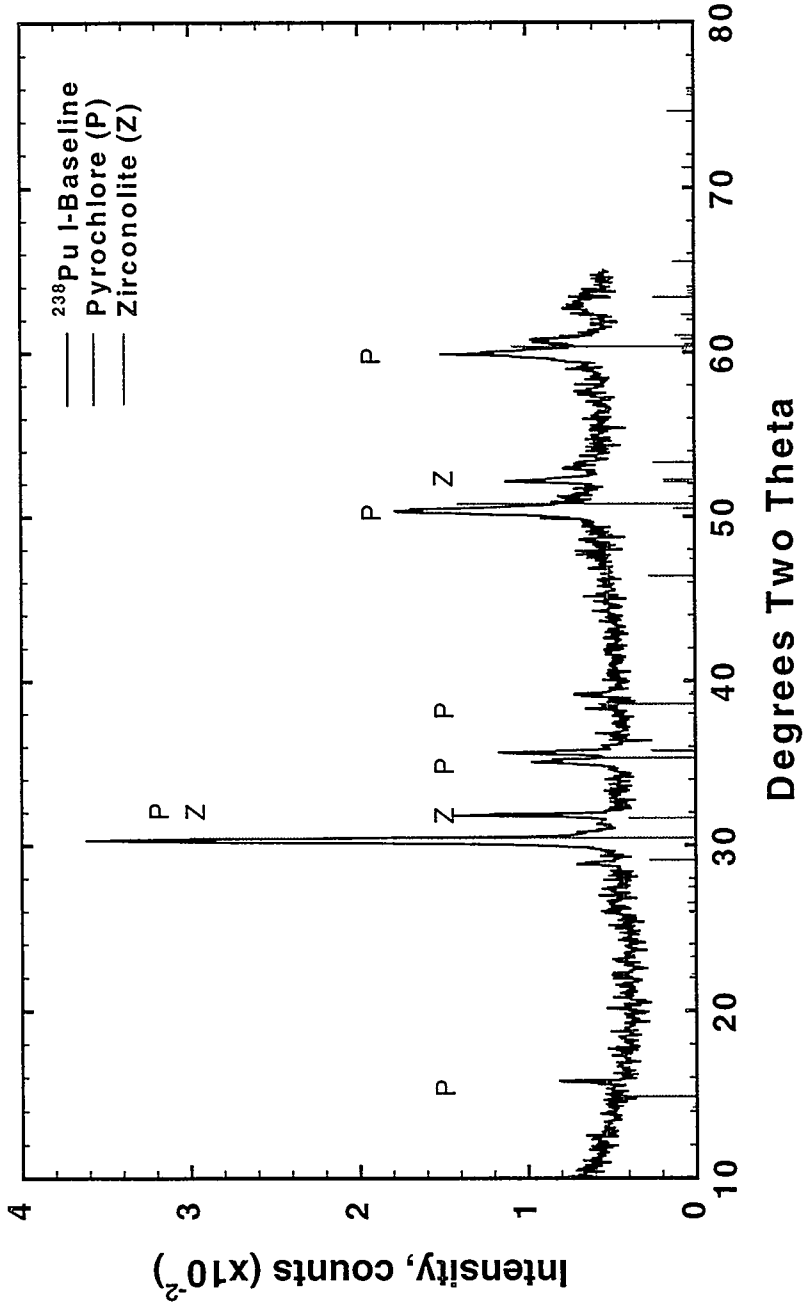

Figure 4.11. Results from the XRD Analysis of ^{238}Pu Impure Baseline

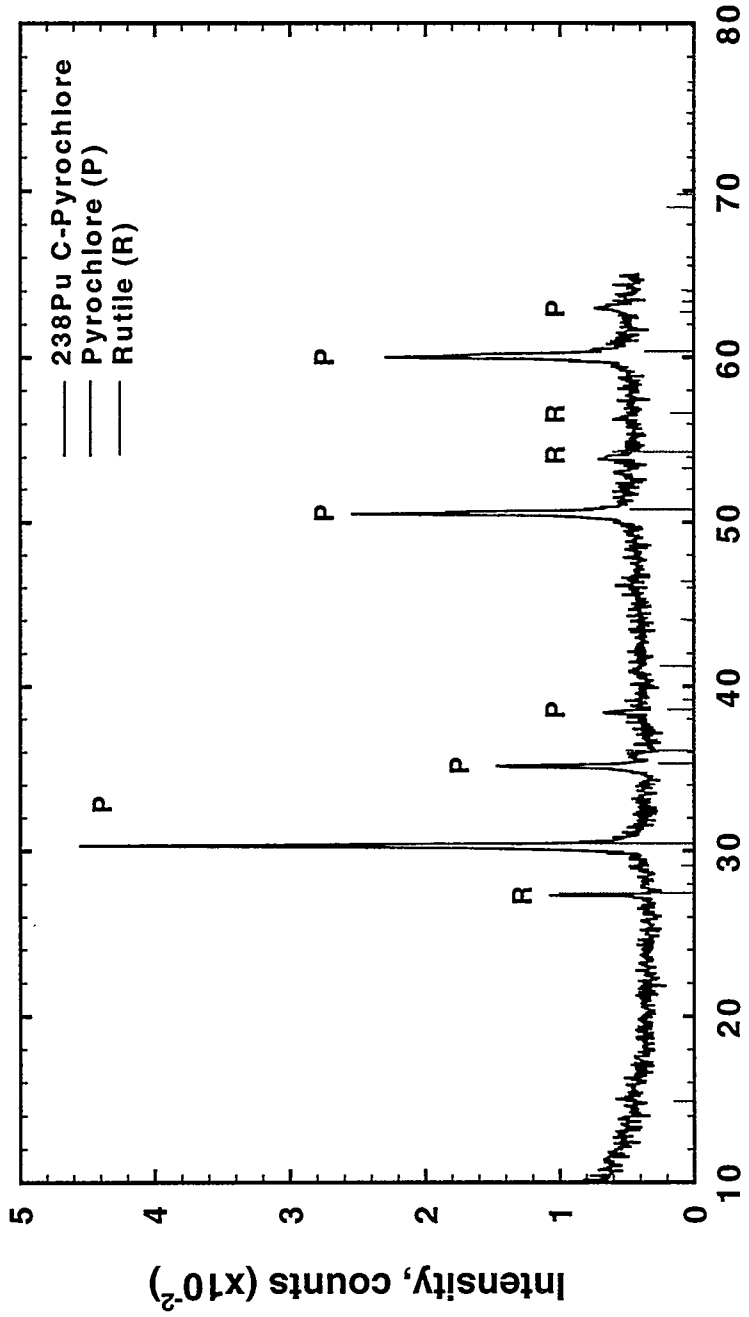

Figure 4.12. Results from the XRD Analysis of ^{238}Pu Coarse Pyrochlore

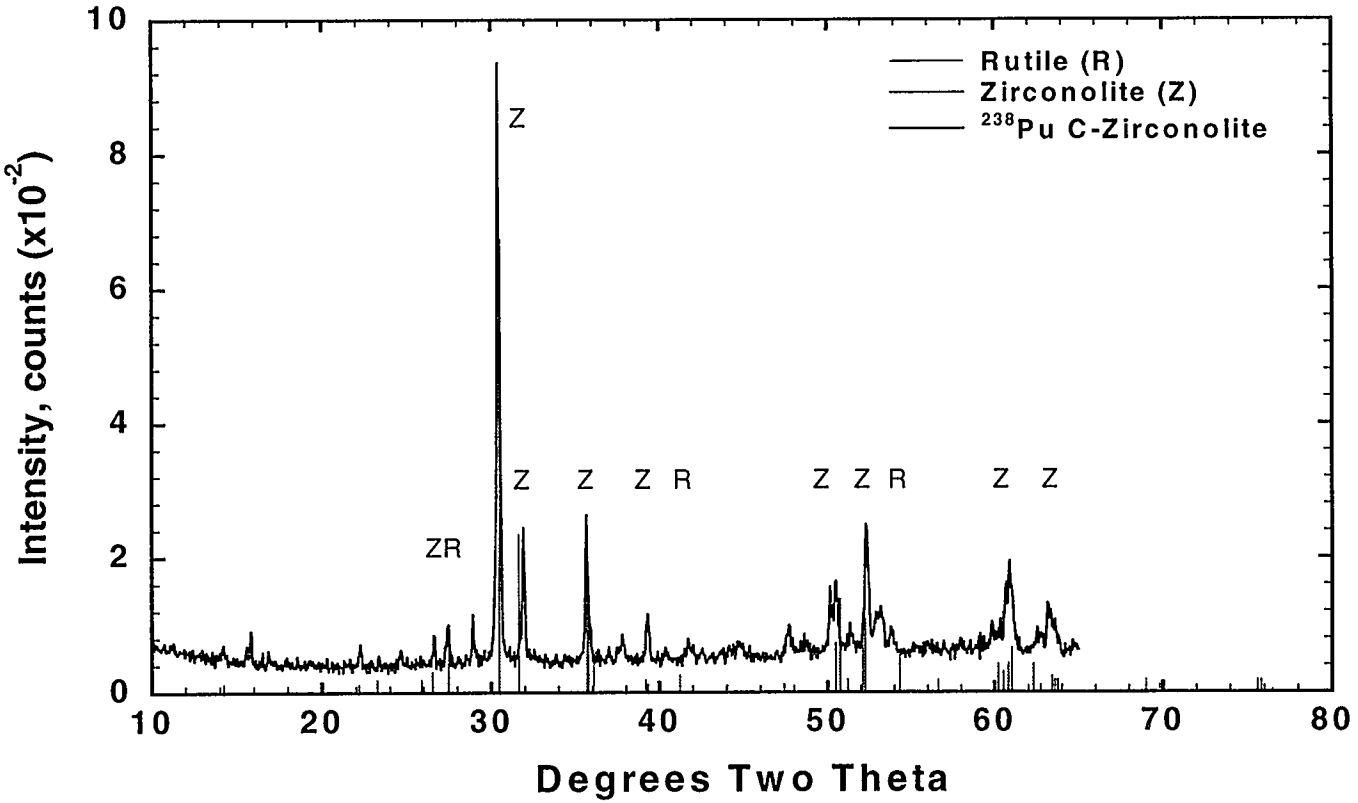

Figure 4.13. Results from the XRD Analysis of ^{238}Pu Coarse Zirconolite

baseline. This material contained substantial amounts of unreacted $^{238}PuO_2$ that resulted because the ^{238}Pu solution partially evaporated between GEA analyses and use (see Figure 4.10). The pyrochlore and zirconolite baseline materials contained brannerite, but no brannerite was detected in the impure baseline material. To check on the reproducibility of the XRD method, the XRD patterns from two ^{238}Pu pyrochlore baseline specimens were obtained. These diffraction patterns were essentially identical in both peak position and intensity.

4.3 Physical Appearance

Photographs of the specimens were obtained by use of a video camera. Some of the best and worst looking specimens are shown in Figure 4.14. In Figure 4.14a, a specimen that is representative of the best-looking specimens is shown. In Figure 4.14b, an average looking specimen is shown. The majority of the specimens are distributed between these two types of pellets. The typical flaw is a chip or minor crack in the surface of the specimen. In Figure 4.14c and d, the worst of the pellets are shown. Of the total number, four appear as shown in Figure 4.14c; the only specimen with the worst appearance is the one shown in Figure 4.14d (^{239}Pu-zirconolite baseline). It is likely that the severe cracking observed for the ^{239}Pu-zirconolite baseline specimens resulted in the very low single pellet density of $4.89 \cdot 10^3$ kg/m^3 compared to the others' average of $5.33(3) \cdot 10^3$ kg/m^3.

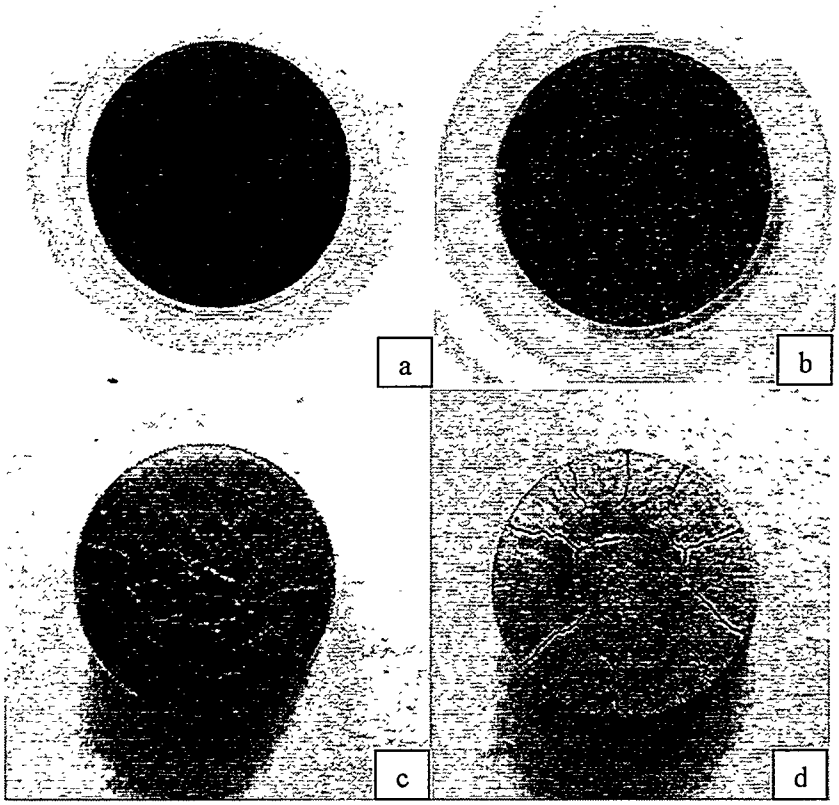

Figure 4.14. Photographs of Representative Specimens. a) Best Looking, b) Average, c) Typical of the Bad Looking, and d) Worst Looking (239Z-Baseline).

Initially, our ^{238}Pu-zirconolite specimens were severely cracked, even though we used a 5°C/min heating rate in their preparation, so we ground the specimens with a mechanical ball mill (Wig-L-Bug), and we remilled, repressed, and resintered them at 1400°C after bringing the temperature up at a slower heating rate (≤2.5°C/min). We did not perform the same operations for the cracked ^{239}Pu-ceramics, such as shown in Figure 4.14d, because we expect no additional radiation damage to the specimens.

4.4 Leach Test Results

The normalized elemental mass loss results for the 3-day MCC leach tests are presented in Table 4.2 (principal components) and Table 4.3 (impurities in the impure baseline specimens). The leaching results are presented as a normalized elemental mass loss in g/m^2 or for the ^{238}Pu as $\mu Ci/m^2$. The measured initial pH of the DIW used as leachate began at ~8 at 21°C; however, the reading drifted steadily down until it stabilized at 7.1 after 1 h. This instability in the pH reading is due to the absence of any ions in the DIW and the slow absorption of carbon dioxide from the air. We omitted the measured values for the pH in this report because they were unreliable because of operational problems that prevented us from measuring pH for about a month after completion of the MCC-1 tests. Note that as you inspect Table 4.2, you will find some negative values that arise from correcting for blanks. This shows that many measured levels are near detection limits.

The elemental releases from the various tested ceramics depended on 1) the element itself, 2) the Pu isotope in the specimens, and 3) the ceramic identity. The following paragraphs summarize the elemental releases observed during the MCC tests of each ceramic. It is worth remembering as you read the following discussion that a first leach test of a new sample can give strange results because of grain-boundary phases and unreacted material. Comparison of MCC test results over time may provide greater insights into the nature of the specimens as radiation damage occurs.

Inspection of the pyrochlore results in Table 4.2 shows that relatively high ($\geq 10^{-2}$ g/m^2 or $\mu Ci/m^2$) amounts of Ca (0.2 g/m^2), ^{238}Pu ($8 \cdot 10^{-3}$ g/m^2, $9 \cdot 10^{-3}$ μCi $^{238}Pu/m^2$), and Mo (4.3 g/m^2 for the ^{239}Pu specimens and 0.06 g/m^2 for the ^{238}Pu specimens) were released in the 3-day MCC test. The amount of Ca released (0.2 g/m^2) was the largest. Only small amounts of the Gd ($2 \cdot 10^{-4}$ and $4 \cdot 10^{-3}$ g/m^2), Hf ($4 \cdot 10^{-5}$ and $4 \cdot 10^{-4}$ g/m^2), and Ti ($3 \cdot 10^{-5}$ and $2 \cdot 10^{-3}$ g/m^2) were released from the ^{239}Pu- and ^{238}Pu specimens, respectively. The releases of Ti from the ^{238}Pu specimens were significantly higher than from the ^{239}Pu specimens, $2 \cdot 10^{-3}$ vs. $3 \cdot 10^{-4}$ g/m^2. There was a significant difference between the behavior of Pu in the ^{239}Pu- and ^{238}Pu specimens with the amount of Pu released from the ^{238}Pu specimens being a factor of 80 greater ($1 \cdot 10^{-4}$ vs. $8 \cdot 10^{-3}$ g/m^2). It is worth noting the close agreement between the ICP/MS-measured Pu ($8 \cdot 10^{-3}$ g/m^2) and the GEA-measured ^{238}Pu ($9 \cdot 10^{-3}$ g/m^2) results for the ^{238}Pu specimen analyses, which provides confidence that the Pu analyses are accurate and that analytical issues can not be used to explain observed differences in observed Pu releases between the ^{238}Pu and the ^{239}Pu specimens. As you review the Pu results for the other ceramics, note that the amounts of Pu measured by these independent analytical methods are consistent. Both sets of specimens released moderate and nearly equal amounts of U in the leach tests ($6 \cdot 10^{-3}$ and $5 \cdot 10^{-3}$ g/m^2). With respect to Mo, the ^{239}Pu specimens lost more (4 g/m^2) than the ^{238}Pu-bearing specimens (0.06 g/m^2). The higher releases of Ti and Pu from the ^{238}Pu specimens suggest that we may already be seeing some radiation-damage effects.

Table 4.2. Leaching Behavior During 3-Day MCC Leach Test of Primary Constituents. Leaching Behavior of Impurities in Baseline with Impurities Samples Presented in Table 4.3.

Ceramic	Normalized Elemental Mass Leached, g/m^2 ($\mu Ci/m^2$)								
	Element (Radioisotope),								
	Al	Ca	Gd	Hf	Ti	Pu	^{238}Pu	U	Mo
239 Pyrochlore	NP	$2.2 \cdot 10^{-1}$	$1.6 \cdot 10^{-4}$	$3.5 \cdot 10^{-5}$	$3.4 \cdot 10^{-5}$	$9.7 \cdot 10^{-5}$	ND	$6.3 \cdot 10^{-3}$	$4.3 \cdot 10^{+0}$
238 Pyrochlore	NP	$2.3 \cdot 10^{-1}$	$(4.5 \cdot 10^{-3})$	$4.2 \cdot 10^{-4}$	$1.6 \cdot 10^{-3}$	$8.0 \cdot 10^{-3}$	$9.3 \cdot 10^{-3}$	$4.6 \cdot 10^{-3}$	$6.4 \cdot 10^{-2}$
239 Coarse Pyrochlore	NP	$2.1 \cdot 10^{-1}$	$3.4 \cdot 10^{-4}$	$-1.4 \cdot 10^{-5}$	$-2.0 \cdot 10^{-4}$	$6.7 \cdot 10^{-5}$	ND	$1.3 \cdot 10^{-3}$	$5.5 \cdot 10^{-2}$
238 Coarse Pyrochlore	NP	$3.3 \cdot 10^{-1}$	$4.4 \cdot 10^{-4}$	$1.6 \cdot 10^{-4}$	$3.3 \cdot 10^{-5}$	$6.1 \cdot 10^{-3}$	$1.1 \cdot 10^{-2}$	$3.7 \cdot 10^{-3}$	$1.8 \cdot 10^{-1}$
239 Pyrochlore Rich Baseline	NP	$7.6 \cdot 10^{-1}$	$2.5 \cdot 10^{-4}$	$-8.7 \cdot 10^{-6}$	$3.3 \cdot 10^{-4}$	$1.8 \cdot 10^{-4}$	ND	$2.1 \cdot 10^{-3}$	$3.5 \cdot 10^{+1}$
238 Pyrochlore Rich Baseline	NP	$1.6 \cdot 10^{+0}$	$3.5 \cdot 10^{-2}$	$1.8 \cdot 10^{-4}$	$3.4 \cdot 10^{-3}$	$2.1 \cdot 10^{-2}$	$2.6 \cdot 10^{-2}$	$2.6 \cdot 10^{-2}$	$7.9 \cdot 10^{+0}$
239 Baseline with Impurities	$4.1 \cdot 10^{+0}$	$4.0 \cdot 10^{-1}$	$2.5 \cdot 10^{-3}$	$-(1.2 \cdot 10^{-5})$	$-1.0 \cdot 10^{-4}$	$5.9 \cdot 10^{-5}$	ND	$1.6 \cdot 10^{-3}$	$4.7 \cdot 10^{+0}$
238 Baseline with Impurities	$1.5 \cdot 10^{+0}$	$1.5 \cdot 10^{+0}$	$2.5 \cdot 10^{-3}$	$(6.7 \cdot 10^{-5})$	$1.9 \cdot 10^{-3}$	$4.5 \cdot 10^{-3}$	$4.5 \cdot 10^{-3}$	$3.1 \cdot 10^{-3}$	$4.1 \cdot 10^{-1}$
239 Zirconolite	$2.0 \cdot 10^{-2}$	$4.7 \cdot 10^{-1}$	$1.0 \cdot 10^{-2}$	$3.4 \cdot 10^{-6}$	$1.1 \cdot 10^{-4}$	$9.0 \cdot 10^{-5}$	ND	$5.3 \cdot 10^{-3}$	$8.9 \cdot 10^{+0}$
238 Zirconolite	$2.2 \cdot 10^{-2}$	$9.4 \cdot 10^{-1}$	$2.4 \cdot 10^{-3}$	$5.7 \cdot 10^{-5}$	$2.1 \cdot 10^{-3}$	$2.3 \cdot 10^{-3}$	$4.0 \cdot 10^{-3}$	$3.1 \cdot 10^{-2}$	$6.5 \cdot 10^{-1}$
239 Coarse Zirconolite	$-(1.5 \cdot 10^{-1})$	$4.3 \cdot 10^{-1}$	$2.7 \cdot 10^{-4}$	$3.3 \cdot 10^{-6}$	$3.0 \cdot 10^{-5}$	$1.2 \cdot 10^{-5}$	ND	$2.1 \cdot 10^{-3}$	$2.9 \cdot 10^{+0}$
238 Coarse Zirconolite	$(3.3 \cdot 10^{-1})$	$4.1 \cdot 10^{-1}$	$1.8 \cdot 10^{-3}$	$(2 \cdot 10^{-5})$	$(1.8 \cdot 10^{-3})$	$3.6 \cdot 10^{-3}$	$4.0 \cdot 10^{-3}$	$2.7 \cdot 10^{-2}$	$(2 \cdot 10^{-1})$
239 Zirconolite Rich Baseline	$1.6 \cdot 10^{-1}$	$6.5 \cdot 10^{-1}$	$5.3 \cdot 10^{-3}$	(0.0)	$1.3 \cdot 10^{-3}$	$2.2 \cdot 10^{-4}$	ND	$1.0 \cdot 10^{-2}$	$2.7 \cdot 10^{+0}$
238 Zirconolite Rich Baseline	$8.1 \cdot 10^{-1}$	$6.8 \cdot 10^{-1}$	$2.4 \cdot 10^{-3}$	$1.9 \cdot 10^{-5}$	$1.5 \cdot 10^{-3}$	$1.4 \cdot 10^{-2}$	$1.2 \cdot 10^{-2}$	$4.3 \cdot 10^{-2}$	$2.4 \cdot 10^{-1}$

NP = Not Present in Material

ND = Not Determined

(###) Indicates below Quantification Limit

Table 4.3. Leach Behavior of Impurities in Baseline with Impurities Specimens

Element	Normalized Amount Leached, g/m^2	
	Material	
	239 Baseline with Impurities	238 Baseline with Impurities
B	$1.2 \cdot 10^{+1}$	$2.9 \cdot 10^{+0}$
Cr (ICP/AES)	$-(2.7 \cdot 10^{-1})$	ND
Cr (ICP-MS)	$1.4 \cdot 10^{-1}$	$1.3 \cdot 10^{-1}$
Fe	$1.4 \cdot 10^{+0}$	$1.5 \cdot 10^{+0}$
Ga	$2.0 \cdot 10^{+0}$	$3.9 \cdot 10^{-1}$
K	$2.4 \cdot 10^{+1}$	$7.6 \cdot 10^{+0}$
Mg	$2.8 \cdot 10^{+0}$	$8.4 \cdot 10^{-1}$
Ni (ICP-AES)	$5.6 \cdot 10^{-1}$	ND
Ni (ICP-MS)	$3.9 \cdot 10^{-1}$	$-6.6 \cdot 10^{-1}$
Na	$-2.0 \cdot 10^{+1}$	$2.2 \cdot 10^{+1}$
Si	$1.5 \cdot 10^{+1}$	ND
Ta	$<0 \cdot 10^{+0}$	$<3 \cdot 10^{-3}$
W	$2.5 \cdot 10^{-2}$	$7.3 \cdot 10^{-3}$
Zn (ICP-AES)	$1.5 \cdot 10^{+1}$	ND
Zn (ICP-MS)	$1.6 \cdot 10^{+1}$	$1.4 \cdot 10^{+2}$
Cl^-	$4.3 \cdot 10^{+1}$	$5.2 \cdot 10^{+1}$
F^-	<0	<0

ND = Not Determined

It is unlikely that the increase in Pu release for these pyrochlores and other, as discussed later, ^{238}Pu-bearing specimens is due to the higher specific activity of ^{238}Pu compared with ^{239}Pu. This is because the recoiling atom would be ^{234}U. The concentration of ^{234}U is expected to be below detection limits for the ICP/MS and was undetectable with GEA. Additionally, if the recoiling atom caused additional matrix atoms to be ejected into solution, including ^{238}Pu, then we would have expected detectable increases in all the primary elements as well. As discussed, no such increase was found.

The behavior of the coarse pyrochlore was similar to that of the pyrochlore with some exceptions. In contrast to the ^{238}Pu-pyrochlore, Ti was not released to any appreciable extent ($3 \cdot 10^{-5}$ g/m^2) from the ^{238}Pu specimens. We again observe that the amount of Pu released from the ^{238}Pu specimens was about a factor of 100 greater than from the ^{239}Pu specimens ($7 \cdot 10^{-5}$ vs. $6 \cdot 10^{-3}$ g/m^2). There is only a factor of 2 difference, likely not a significant difference, in the amount of Mo released from the two specimens; in this instance, more is removed from the ^{238}Pu specimens. As with the pyrochlore, the difference between the amounts of Pu leached from the ^{239}Pu specimens ($7 \cdot 10^{-5}$ g/m^2) and the amount of Pu released from the ^{238}Pu specimens (0.6 to $1 \cdot 10^{-2}$ g/m^2) suggests that some radiation damage may have occurred.

The amounts released from the pyrochlore-rich baseline specimens are higher compared to the phase-pure pyrochlore. Relatively large amounts of the Ca (0.8 g/m^2) and Mo (35 g/m^2) were released from the ^{239}Pu specimens while significant amounts of Ca (1.6 g/m^2), Gd ($4 \cdot 10^{-2}$ g/m^2), Pu (0.02 g/m^2), U (0.03 g/m^2), and Mo (8 g/m^2) were released from the ^{238}Pu specimens. As with the pyrochlore and the coarse pyrochlore, the Pu amount removed is about a factor of 100 higher from the ^{238}Pu specimens (0.02 g/m^2) than from the ^{239}Pu specimens ($2 \cdot 10^{-4}$ g/m^2). The relative Gd amounts released are similar to the relative Pu releases ($3 \cdot 10^{-4}$ vs. $4 \cdot 10^{-2}$). The amounts of U and Ti released are a factor of 10 higher from the ^{238}Pu specimens. The fraction of Mo leached is a factor of 10 higher from the ^{239}Pu specimens.

Inspection of Table 4.2 and Table 4.3 show that the ^{239}Pu and ^{238}Pu- baseline with impurities specimens (respectively) lost significant amounts of their Al (4 and 2 g/m^2), Ca (0.4 and 2 g/m^2), Mo (5 and 0.4 g/m^2), and the impurities with the exception of Ta. As with all the other specimens, the amount of Pu released is about a factor of 100 greater from the ^{238}Pu specimens.

Relatively large amounts of Al (0.02 g/m^2), Ca(0.5 g/m^2), Gd (0.01 g/m^2), and Mo (9 g/m^2) were released from the ^{239}Pu-zirconolite specimens and relatively large amounts of Al (0.02 g/m^2), Ca (0.9 g/m^2), U (0.03 g/m^2), and Mo (0.6 g/m^2) were released from the ^{238}Pu-zirconolite specimens during the MCC leach test. The amount of Al released was the same for both sets of duplicate specimens. The Ca releases from the ^{239}Pu- and ^{238}Pu specimens are within a factor of 2 of each other. The amount of Gd released from the ^{239}Pu specimens is a factor of 5 greater than from the ^{238}Pu specimens. The Hf and Ti releases from the ^{238}Pu specimens ($6 \cdot 10^{-5}$ and $2 \cdot 10^{-3}$ g/m^2) are nearly a factor of 20 greater than the releases from the ^{239}Pu-specimens ($3 \cdot 10^{-6}$ and $1 \cdot 10^{-4}$ g/m^2). The Pu release from the ^{238}Pu specimens ($2 \cdot 10^{-3}$ g/m^2 and $4 \cdot 10^{-3}$ μCi ^{238}Pu $/m^2$) is between 20 to 40 times greater than from the ^{239}Pu specimens ($9 \cdot 10^{-5}$ g/m^2). The U released from the ^{238}Pu specimens is about 6 times greater than from the ^{239}Pu specimens ($5 \cdot 10^{-3}$ g/m^2). The amount of Mo released from the ^{239}Pu specimens is about a factor of 10 greater than from the ^{239}Pu specimens. The overall leach results suggest that the ^{238}Pu-zirconolite specimens are less resistant to release than the ^{239}Pu-zirconolite specimens.

In general, the coarse zirconolite specimens retained a greater fraction of the contained elements compared to the zirconolite. A significant amount of the Ca was released (0.4 g/m^2), nominally the same as from zirconolite, and was independent of the Pu isotope in the ceramic. The Gd released from the ^{238}Pu specimens was nearly a factor of 10 more, $3 \cdot 10^{-4}$ g/m^2 for the ^{239}Pu specimens vs. $2 \cdot 10^{-3}$ g/m^2 for the ^{238}Pu specimens. The amount of Hf removed was small ($3 \cdot 10^{-6}$ g/m^2). The Ti released from the ^{238}Pu specimen ($2 \cdot 10^{-3}$ g/m^2) was greater than that from the ^{239}Pu specimen ($3 \cdot 10^{-5}$ g/m^2), although the amount measured for the ^{238}Pu specimens was below the quantification limit for the ICP/MS. Again, the Pu released from the ^{238}Pu specimens ($4 \cdot 10^{-3}$ g/m^2 and $4 \cdot 10^{-3}$ μCi $^{238}Pu/m^2$) was greater than the amount released from the ^{239}Pu specimens ($1 \cdot 10^{-5}$ g/m^2) by a factor of 100. The amount of U released from the ^{238}Pu-coarse zirconolite ($3 \cdot 10^{-2}$ g/m^2) was a factor of 10 greater than from the ^{239}Pu specimen ($2 \cdot 10^{-3}$ g/m^2). The Mo was again higher in the leachates from the ^{239}Pu specimen (3 vs. 0.2 g/m^2). The MCC leach test results indicate that several of the constituents in the ^{238}Pu-coarse zirconolite are more easily released than from the ^{239}Pu-coarse zirconolite.

Relatively large amounts of Al (0.2 g/m^2), Ca (0.6 g/m^2), U (0.01 g/m^2), and Mo (35 g/m^2) were released from the ^{239}Pu zirconolite-rich specimens, and relatively large amounts of Al (0.8 g/m^2), Ca (0.7 g/m^2), Pu (0.01 g/m^2, 0.01 μCi $^{238}Pu/m^2$), U (0.04 g/m^2), and Mo (0.2 g/m^2) were released from the ^{238}Pu specimens. The Al release from the ^{238}Pu specimens was a factor of 4 greater than from the ^{239}Pu-zirconolite-rich baseline specimens. The Ca and Ti releases were the same for each of the sets of Pu specimens. The Gd releases were slightly higher than from the ^{239}Pu specimens ($5 \cdot 10^{-3}$ vs. $2 \cdot 10^{-3}$ g/m^2) and probably do not reflect a true difference in behavior. Again, the Pu release from the ^{238}Pu specimens (0.01 g/m^2) was nominally a factor of 50 greater than from the ^{239}Pu specimens ($2 \cdot 10^{-4}$ g/m^2). Nearly the same U release occurred for both sets of specimens; the amount removed from the ^{238}Pu specimens was a factor of 4 higher. More Mo was released from the ^{239}Pu specimens (3 g/m^2) than from the ^{238}Pu specimens (0.2 g/m^2). The MCC leach test of the zirconolite-rich baseline specimens suggests that some of the constituents in the ^{238}Pu-bearing material are more easily released than in the analogous ^{239}Pu-material. Because the ^{239}Pu specimens are cracked, their actual surface area will be higher than their geometric surface area calculated based on their height and diameter. Use of the geometric surface area of a highly fractured specimen will result in a higher release rate than if the higher surface area were used. However, comparison of the ^{239}Pu specimen results with the unfractured ^{238}Pu specimens shows similar behaviors for those elements released in relatively large amounts.

At this time, we do not understand the higher Pu releases from the ^{238}Pu specimens than from the ^{239}Pu specimens. Although radiation damage effects could cause these increases, it is unlikely because of the short time between production and testing. Atom recoil and the higher activity of ^{238}Pu relative to ^{239}Pu cannot be used to explain the difference as discussed above. The high specific activity at the surface of these specimens could cause oxidizing conditions to promote Pu(IV) to Pu(V), which is more soluble. However, U(IV) would also be oxidized to U(VI) with a concomitant increase in solubility. The consistent results between the ICP/MS-measured Pu and the GEA-measured ^{238}Pu indicate that analytical problems are not the cause of these differences.

With all the difficulties of working with this number of ^{238}Pu-bearing specimens, the pH measurements were not made for about a month. As a result, the values that were measured were consistent with the pH of water saturated with CO_2 at ambient conditions [$\log(P_{co2}) = -3.5$; $pH \approx 5$]. This result is generally consistent with the analytical results that show the solutions to have very few dissolved solids.

To test this hypothesis, the analyzed chemical composition of a solution from one of the ^{239}Pu-pyrochlore specimens (239Pyro18-6) was input into the EQ3/6 geochemical code [16]. The calculation was carried out by assuming that the $CO_2(g)$ equilibrates with solution at 90°C at a pH of 7. Sodium ion was used to make up for any electrical imbalance in the solution due to analytical errors. To achieve electric balance, 470 ppb Na^+ was added to the solution. The temperature of this resulting solution was lowered to 25°C with the amount of HCO_3^- calculated to result from equilibrium with $CO_2(g)$ at 90°C ($1.67 \cdot 10^{-5}$ molal). If the Na^+ is left at 470 ppb, the resulting calculated pH is 8.5. However, the analyzed concentration of Na is less than the detection limit, implying that the value should be around 20 ppb. With this amount of Na^+ in solution, the newly calculated pH is 5.4. The conclusion from these

calculations is that the ion balance from the analytical laboratory is quite good and the range of possible pH values is what has been reported by other laboratories [17, 18, 19]. In fact, even though the pH values we measured were deemed to be unreliable, they may have been the correct values. We will be able to determine this when the next set of tests is run, when we plan to measure the pH values immediately after the test ends. If those pH values are similar to the ones measured this time, then the current values are probably good despite the long storage time.

The geochemical calculations also predict the solid mineral phases with which the solution would be in equilibrium. These phases are discussed briefly here. While $Fe(OH)_3$ was calculated to be saturated at 90°C, it was undersaturated at 25°C. While rutile and PuO_2 were calculated to be supersaturated at both temperatures, other phases, including Ti or Pu, were not. Soddyite [$(UO_2)_2SiO_4 \cdot H_2O$], nontronite clays, and goethite [FeOOH] were also listed as phases that were saturated or supersaturated. Gibbsite [$Al(OH)_3$] was found to be saturated at 25°C and pH 8.5, but not at 90°C and not at 25°C, and a pH of 5.4.

One experimental note to be made is on the method for making pH measurements in these solutions with low dissolved solids (ionic strength of about $1 \cdot 10^{-6}$ molal). When the ionic strength of the solution is this low, the junction potential for the pH probe becomes unstable. Drift in the meter reading becomes a real problem. This was corrected for our measurements by making the aliquot used for pH measurement about 1 mM NaCl. This was done by adding a small volume (50 to 100 μL) of a concentrated solution of NaCl to the aliquot. The stock solution was made with demineralized water and high purity, optical grade NaCl. For this use, reagent grade NaCl cannot be used because there is just enough un-neutralized base in the salt to raise the pH of the solution. Potassium chloride may also be used, but it also must be high purity, optical grade.

5.0 Conclusions

The results from this initial characterization of the ^{238}Pu- and ^{239}Pu-bearing ceramics showed that the target phase assemblage was achieved in all but one material, ^{238}Pu-zirconolite baseline. This ^{238}Pu-zirconolite baseline material appears to have been prepared incorrectly with a 14 mass% excess of Pu (9.6 mass% actual vs. 8.4 mass% target; 4.8 mole% actual vs. 4.1 mole% target). It is not surprising that PuO_2 was found to be one of the dominant phases. The densities of these materials compared well with the theoretical densities given by Stewart, Vance, and Ball [14]. For all but three of the materials, the average density was >94% of theoretical. Of the three, one was ^{238}Pu-zirconolite baseline (108%) that contained unreacted PuO_2.

In our MCC leach testing, the normalized elemental mass losses from the various ceramic specimens depended on the elemental ceramic constituent, the Pu isotope, and the ceramic. Of the primary constituents, Al and Ca were the most easily released. Plutonium and U were the next most susceptible to release. In general, the Hf had the lowest releases during the tests. The Gd and Ti releases varied, depending on the ceramic and the Pu isotope in the ceramic. The Mo, which was added as a trace constituent to monitor the stability of the crystalline structure, exhibited consistently high-normalized elemental releases.

The amount of Pu leached depended the most on the Pu isotope in the ceramic with more Pu released from the ^{238}Pu specimens than from the ^{239}Pu specimens, independent of ceramic type. Interestingly, the Mo releases were typically higher for the ^{239}Pu specimens than for the ^{238}Pu specimens. The higher Pu release from the ^{238}Pu specimens is not yet understood; the consistency between the ICP/MS- and GEA-measured Pu releases from the ^{238}Pu specimens eliminates analytical problems as an explanation.

With respect to the effects of ceramic type, the three baseline ceramics often had the highest releases. The highest Pu releases were from the pyrochlore-rich and zirconolite-rich baselines. The highest U releases were from the pyrochlore-rich and zirconolite-rich baselines and zirconolite.

Values for the pH of the leachates were deemed unreliable because of the length of time between the end of the test and the measurement. This resulted in pH values that were consistent with CO_2-saturated water at ambient conditions. However, initial calculations with EQ3/6 suggest that the measured pH values are to be expected, given the solution concentrations and the assumptions that went into the calculations.

6.0 References

1 U.S. Department of Energy (DOE). 1996. *Storage and Disposition of Weapons-Usable Fissile Materials Final Programmatic Environmental Impact Statement*, Washington, DC.

2 62 FR 3014. January 14, 1997. U.S. Department of Energy. "Fissile Materials Storage and Disposition Programmatic Environmental Impact Statement Record of Decision, Storage and Disposition Final PEIS," *Federal Register*.

3 R. Devanathan, W. J. Weber, and L. A. Boatner. 1998. "Response of Zircon to Electron and Ne^{+} Irradiation." In *Materials Research Society Symposium Proceedings*, 481, Materials Research Society, Pittsburgh, Pennsylvania.

4 TRW Environmental Safety Systems Inc. 1997. *Degraded Mode Criticality Analysis of Immobilized Plutonium Waste Forms in a Geologic Repository,* A00000000-01717-5705-00014 REV 01, Las Vegas, Nevada.

5 A. Meldrum, S. J. Zinkle, and L. A. Boatner. 1999. "Heavy-ion Irradiation Effects in the ABO_4 Orthosilicates: Decomposition, Amorphization, and Recrystallization," *Physical Review B* 59(6).

6 S. X. Wang, L. M. Wang, R. C. Ewing, G. S. Was, and G. R. Lumpkin. 1999. "Ion irradiation-induced phase transformation of pyrochlore and zirconolite," *Nucl. Instr. Methods Phys. Res. B* 148, pp 704–709.

7 K. L. Smith, M. G. Blackford, G. R. Lumpkin, and N. J. Zaluzec. 2000. "Temperature Dependence of Ion Irradiation Induced Amorphisation of Zirconolite." In *Scientific Basis for Nuclear Waste Management XXIII*, Materials Research Society, Warrendale, Pennsylvania.

8 S. X. Wang, L. M. Wang, R. C. Ewing, and K. V. Govidan Kuttty. 2000. "Ion Irradiation Effects for Two Pyrochlore Compositions: $Gd_2Ti_2O_7$ and $Gd_2Ti_2O_7$." In *Scientific Basis for Nuclear Waste Management XXIII*, Materials Research Society, Warrendale, Pennsylvania.

9 S. X. Wang, B. D. Begg, L. M. Wang, R. C. Ewing, W. J. Weber, and K. V. Govidan Kuttty. 1999. "Radiation stability of gadolinium zirconate: A waste form for plutonium disposition," *J. Materials Research*, 14(12), pp 4470-4473.

10 B. B. Ebbinghaus, C. Cicero-Herman, L. Gray, and H. Shaw. 1999. *Baseline Formulation*, UCRL-ID-133089, Lawrence Livermore National Laboratory, Livermore, CA.

11 American Society for Testing and Materials (ASTM) C1220. 1998. *Standard Method for Static Leaching of Monolithic Waste Forms for Disposal of Radioactive Waste,* C 1220-98, West Conshohocken, Pennsylvania.

12 B. D. Begg, W. J. Weber, R. Devanathan, J. P. Icenhower, S. Thevuthasan, and B. P. McGrail, "Heavy-Ion Irradiation Effects in Pyrochlores," in *Waste Management Science and Technology in the Ceramic and Nuclear Industries*, edited by G. L. Smith, G. T. Chandler, and B. Mobasher (The American Ceramic Society, Westerville, Ohio, 2000) in press.

13 B. P. McGrail, P. F. Martin, J. P. Icenhower, H. T. Schaef, V. L. Legore, and R. D. Orr. *Evaluation of the Long-Term Performance of Titanate Ceramics for Immobilization of Excess Weapons Plutonium: Results From Pressurized Unsaturated Flow and Single Pass Flow-Through Testing.* PNNL-12240, Rev. 0, Pacific Northwest National Laboratory, Richland, Washington.

14 M.W.A. Stewart, E. R. Vance, and C. J. Ball. 1999. *Report on Task 2.3: Physical Properties Measurement,* Australian Nuclear Science and Technology Organisation, Sydney, Australia, September 7.

15 H.F. Shaw. 1998. Determination of the open and closed porosity in an immobilized Pu ceramic waste form, UCRL-ID-132605, Lawrence Livermore National Laboratory, Livermore, CA.

16 Wolery, T.J. 1983. EQ3NR A Computer Program for Geochemical Aqueous Speciation-Solubility Calculations: User's Guide and Documentation. UCRL-53414. Lawrence Livermore National Laboratory, Livermore, CA.

17 A. J. Bakel, C. J. Mertz, M. K. Nole, and D. B. Chamberlain. 1999. *Corrosion Behavior of Titanate Ceramics in Short-term MCC-1 Tests: Results from Tests with Zirconolite-rich, Baseline, and Impurity Ceramics (Milestone 4.1.b)*, PIP-99-102, Lawrence Livermore National Laboratory, Livermore, California.

18 A. J. Bakel, 1999. *Characterization and Corrosion Behavior of Hafnium-Cerium-Uranium Ceramics Containing Impurities (Milestone 4.1.f)*, PIP-99-077, Lawrence Livermore National Laboratory, Livermore, California.

19 C. L. Crawford, C. R. Biddle, and N. E. Bibler. 1999. *Durability Testing of Heavy-Ion-Irradiated Crystalline Ceramics (Milestone 4.1.a)*, PIP-99-100, Lawrence Livermore National Laboratory, Livermore, California.

Distribution

No. of Copies

OFFSITE

2 DOE/Office of Scientific and Technical Information

3 L. Jardine
Lawrence Livermore National Laboratory
P.O. Box 808, L-195
Livermore, CA 94551

Dr. Werner Lutze
University of New Mexico
209 Farris Engineering Building
Albuquerque, NM 87131

Dr. Rodney Ewing
University of Michigan
Geological Sciences
1006 C C Little
Ann Arbor MI
48109-1063

L. A. Boatner
Oak Ridge National Laboratory
PO Box 2008
Oak Ridge, TN 37831-6056

S. G. Johnson
Argonne National Laboratory
P.O. Box 2528
Idaho Falls, ID 83403-2528

R. G. Haire
Oak Ridge National Laboratory
PO Box 2008
Oak Ridge, TN 37831-6375

No. of Copies

FOREIGN

B. Grambow
Ecole de Mines de Nantes
Laboratoire SUBATECH
4 Rue Alfred Kastler
F 44307 Nantes Cedex 3.
FRANCE

A. Jostsons
Australian Nuclear Science and Technology Organization
New Illawarra Road
Lucas Heights
NSW 2234
AUSTRALIA

E. R. Vance
Australian Nuclear Science and Technology Organization
New Illawarra Road
Lucas Heights
NSW 2234
AUSTRALIA

G. R. Lumpkin
Australian Nuclear Science and Technology Organization
New Illawarra Road
Lucas Heights
NSW 2234
AUSTRALIA

No. of
Copies

FOREIGN

L. Nachmilner
Nuclear Research Institute
CZ 250 68 Řež
CZECH REPUBLIC

K. Spahiu
SKB
Box 5864
102 40 Stockholm
SWEDEN

Hj. Matzke
European Commission
Joint Research Center
Institute for Transuranium Elements
Postfach 2340, D-76125 Karlsruhe
GERMANY

T. Wiss
European Commission
Joint Research Center
Institute for Transuranium Elements
Postfach 2340, D-76125 Karlsruhe
GERMANY

B. D. Begg
Australian Nuclear Science and
Technology Organization
New Illawarra Road
Lucas Heights
NSW 2234
AUSTRALIA

No. of
Copies

ONSITE

2 **DOE Richland Operations Office**

D. L Biancosino	K8-50

35 **Pacific Northwest National Laboratory**

J. Abrefah	P7-27
B. O. Barnes	P8-50
W. C. Buchmiller	K6-24
R. J. Elovich	P7-25
B. D. Hanson	P7-25
J. P. Icenhower	K6-81
D. E. Knutson	P7-25
S. C. Marschman	P7-27
B. P. McGrail	K6-81
L. M. Peurrung	K6-24
M. J. O'Hara	K6-81
H. T. Schaef	K6-81
R. D. Scheele (5)	P7-25
R. L. Sell	P7-25
D. M. Strachan (10)	K6-24
J. D. Vienna	K6-24
W. J. Weber	K2-44
Information Release Office (5)	K1-06